A STRUCTURAL PREDICTION OF COPPER SULFIDE AND STUDY OF ITS ELECTRONIC PROPERTIES AND VACANCY FORMING TREND USING DENSITY FUNCTIONAL THEORY

by

PRASHANT KHATRI

Presented to the Faculty of the Graduate School of
The University of Texas at Arlington in Partial Fulfillment
of the Requirements
for the Degree of

MASTERS OF SCIENCE IN PHYSICS

THE UNIVERSITY OF TEXAS AT ARLINGTON

August 2014

Acknowledgements

I would like to thank my advisor, Dr. Muhammad N. Huda, for his great guidance and support, and for giving me an opportunity to work on this project. I am also thankful to Dr. Qiming Zhang and Dr. Raymond Atta-Fynn for showing interest on my research work and serving on my committee.

I would also like to thank my research group members for being helpful and co-operative during my research. Their suggestion and discussion during our group meeting has helped me to understand science more. Especially I would thank Pranab Sarkar and Cedric Mayfield for their help.

I am very grateful to my parents and sibling for allowing me to study abroad to get higher education and for their support and encouragement during my entire academic career. And special thanks go to all my friends who encourage me to work hard and have faith on me.

Finally, I would also like to acknowledge National Renewable Energy Laboratory for funding this research work.

July 18, 2014

Abstract

A STRUCTURAL PREDICTION OF COPPER SULFIDE
AND STUDY OF ITS ELECTRONIC PROPERTIES
AND VACANCY FORMING TREND USING
DENSITY FUNCTIONAL THEORY

Prashant Khatri, MS

The University of Texas at Arlington, 2014

Supervising Professor: Muhammad N. Huda

The focus of this research is on the material challenges in photovoltaic. Copper Sulfide (Cu_2S) has been regarded as a potential solar absorber materials in photovoltaic industry. Despite its simple composition, it is a complex material. Copper atoms are mobile in Cu_2S crystals facilitating copper vacancies; hence promote Cu-deficient non-stoichiometric Cu_xS. Majority of the present work is directed towards understanding the stability issue related with Cu_2S/Cu_xS. We used density functional theory systematically to predict acanthite like structure as ground state structure of Cu_2S. The crystal structure of acanthite Cu_2S is much simpler than the experimentally observed low chalcocite, though electronic structures are similar with Cu-d showing high dominance in valence band. Theoretically we find that both structures show a tendency of forming Cu-vacancy. As it becomes p-type with Cu vacancy, band gap also increases. To understand about the effect of doping in Cu_2S, tin and oxygen doping have been studied.

Table of Contents

List of Illustrations

List of Tables

Chapter 1

Introduction

1.1 Photovoltaic

Photovoltaic (PV) is a method of generating electrical power by converting solar radiation into electricity using semiconductors exhibiting photovoltaic effect. The term “photo” means light and “voltaic” means electricity. Therefore, a PV cell or solar cell is a device made up of semiconductor that generates electricity when light falls on it. The photovoltaic effect was first observed by Alexandre-Edmond Becquerel in 1839 [1, 2] however it was not well studied until the development of quantum theory of light and solid state physics. Although photovoltaic was initially used to power orbiting satellites and other spacecraft [3], now it is being widely use in electric power generation. Solar photovoltaic power generation is a clean sustainable renewable energy technology [4]. Photovoltaic systems have been in used for more than fifty years [5] and this industry is growing at alarming rate. In 2013, it shows a growth of almost 38 percentages with China, Japan and USA are among the fastest growing markets while Germany remains the world largest producer [6, 7].

Developers of photovoltaic device can use a suitable material that can store energy to produce industrial heat or generate electricity. In theory it is a very simple idea but in practical, there are many challenges in photovoltaic. The first challenge is to find a proper material to be used in photovoltaic device. The material needs to have suitable band gap with high stability which can produce photovoltaic effect. Currently most of the PV materials are Silicon based. We will discuss about PV materials in next section. High manufacturing cost of PV cells, stability of material used and relatively low efficiency of PV cells as compared with other sources such as fossil fuels are major barriers in adoption of PV system. So it is important to look for alternative cost effective materials to

be used in photovoltaic. At the same time a proper study and engineering work is needed to be done to improve the energy conversion of the material and improved the durability and product life.

1.2 PV Materials

PV cells are made of semiconductor materials. The types of material used in solar cell applications are crystalline and thin film materials.

1.2.1 Crystalline Materials

Crystalline materials that are mainly used in PV devices are single crystalline silicon, polycrystalline silicon and Gallium Arsenide.

A single crystalline silicon has a uniform molecular structure. As compared with non-crystalline material, the uniformity in crystalline material makes it highly efficient. The conversion efficiency for single-silicon ranges between 15-24% [8]. Single crystalline material is efficient as well as highly reliable for outdoor application. Polycrystralline silicon consists of small grains of single-crystal silicon. The grain boundaries in polycrystalline silicon obstruct the flow of electrons and decrease the power output. Hence, polycrystalline PV cells are energetically less efficient than single-crystalline silicon PV cells. The advantages of using polycrystalline silicon over single crystalline silicon are it is stronger and it is slightly lower in cost with less growth requirements [9]. GaAs is another important semiconducting material in solar cell industry. Its structure is similar to that of silicon and it has a high level of light absorptivity. GaAs has a much higher energy conversion efficiency than crystal silicon and high heat resistance as well [10]. Thus making it ideal for space applications where strong resistance heat damage

and high cell efficiency are required. The main disadvantage of GaAs is the high cost of the single-crystal substrate that GaAs is grown on.

1.2.2 Thin Film Materials

A thin semiconductor layer of PV materials is deposited on low-cost supporting layer such as glass, metal or plastic foil to make a thin film PV material. The manufacturing process is faster, uses less energy and mass production is made easier than the manufacturing process of crystalline silicon and hence thin film materials are cost effective and at the same time have higher light absorptivity than crystalline materials [11]. The major drawback of thin film materials is its poor cell conversion efficiency due to non-single-crystal structure [12]. Materials that are highly used in thin PV cells are amorphous silicon (a-Si), Cadmium Telluride (CdTe), Copper Indium Diselenide (CuInSe2, or CIS).

1.3 Sulfides

Sulfide is an inorganic anion of sulfur. It has an oxidation state of -2. Many important metallic ores contains sulfides [13] such as argentite (silver sulfide), galena (lead sulfide), molybdenite (molybdenum sulfide), sphalerite (zinc sulfide), pyrite (iron disulfide), and chalcopyrite (iron-copper sulfide). Inorganic sulfides typically have very low solubility in water and they are mainly classified as strong base. Bonding in transition metal sulfides is highly covalent which gives rise to semiconductor properties such as Ag_2S [14]. Many transition metallic sulfides are also being used in solar cells as their structural and electronic properties are favorable for being used in PV cells [15].

1.4 Copper Sulfide (Cu_2S)

Copper Sulfide (Cu_2S) has a simple composition, consisting of two Cu atoms and one sulfur atoms in a primitive cell, but is a complex material. This material has been a long term interest in scientific world though the results are somewhat controversial. Structural complexity is one of the main challenges to deal with when studying copper sulfide. The positions of Cu within the sub-lattice of S atoms are not well known. Some suggest coppers are mobile in nature in Cu_2S due to which it can occupy various types of interstitial sites with a statistical distribution depending on temperature [16]. Due to this complex atomic distribution, the understanding of electronic structure is convoluted. Experimental results so far have shown that stoichiometric Cu_2S mainly exists in three forms: monoclinic phase (low chalcocite) formed at temperature below 104^0C, hexagonal phase (high chalcocite) formed between 104-436^0C, and cubic phase which is formed at temperature 436^0C or higher [17, 18]. The three different phases of Cu_2S not only have different geometry but also have different arrangement of coppers. Experimental papers have also reported various structures with different concentration of copper that exist in mineral form. Table 1-1 provides name of the compound that are experimentally identified with their composition [17 – 20]. Most of the study conducted so far on copper sulfide report semiconducting nature of these compounds. Energy gaps from 1.1 eV to 1.5 eV have been reported from experimental works with both direct and indirect transitions for Cu_xS [17 - 22]. From the first principle theory point of view, not much has been published on copper sulfide [23, 24].

Table 1 Name of Cu_xS

X	Name
2	Chalcocite [17, 18]
1.94-1.96	Djurleite [17, 18]
1.8	Digenite [19]
1.75	Anilite [20]

Copper Sulfides are important in solar industry as it is an interesting semiconductor and has a band gap of around 1.21 eV [25] which is suitable for the photovoltaic (PV) applications. To replace single crystalline silicon with low cost and high performance materials [26], a thin film of semiconductors such as Cu_2S/CdS presents viable alternatives [27, 28]. The use of Cu_2S/CdS gave around 9-10% efficiency in the past but it suffered from deterioration in air due to strong oxidizing agent O_2 [23, 24, 29, 30]. In Cu_2S/CdS heterojunctions, the photoresponse is due to light absorption in the Cu_2S followed by electron diffusion to the Cu_2S-CdS interface [31]. However, the heterojunction of Cu_2S/CdS is complicated that causes defect states near the interface causing Cu diffusion into the CdS [32]. Reference [33] describes the problem related with Cu_2S/CdS application in solar cells, one of them is cell stability problem which is mainly caused by mobile nature of copper in Cu_2S. This instability leads to copper precipitation resulting in vacancy in Cu_2S. Hence, a major problem in Cu_2S is the copper atom's instability towards the formation of copper vacancy [23, 24, 29, 30]. Due to this mobile nature of Cu and vacancy forming trend in cuprous sulfide, the efficiency of the cell decreases and its uses in solar industry as well.

Copper sulfide is again gaining considerable interest due to the development of nano technology. Many scientists are working in the field of nanotechnology in growing

Cu_2S/Cu_xS nanocrystals for solar cells and other applications [34, 35], even for the field of medicine. As solar cells and medical fields are two important and highly emerging fields, it is necessary to have proper theoretical understanding of Cu_2S/Cu_xS.

The organization of thesis is as follows. In chapter 2, we present a brief description of the methodology on which our calculation is based- a quantum mechanical based calculation called density functional theory. We also describe about computational scheme in chapter 2. In chapter 3, we explained how we determine lowest energy ground state stoichiometry structure for Cu_2S and then focus on studying the structural and electronic properties of Cu_2S. Chapter 4 is devoted to Cu_2S structure with copper vacancy on them. In chapter 5 we discuss about doping in Cu_2S. Finally in chapter 6, we summarize our findings and propose some future work needed to be done on Cu_2S.

Chapter 2

Methodology

Quantum Mechanics was developed in early twentieth century to solve the problem which cannot be described by classical mechanics. In our study we use density functional theory, a quantum mechanical based calculation, as the theoretical framework of our calculations. We carry them out using projected augmented wave (PAW) method using a Vienna Abinitio Simulation Package (VASP).

2.1 Problem of Many-Body System

One of the basic problems in many areas of theoretical physics and chemistry is finding the ground state properties of many atom system. First we need to solve Schrodinger equation

$$H\Psi(R,r) = E\Psi(R,r) \tag{2.1}$$

where H is the Hamiltonian and Ψ(R,r) is the wavefunction of the system. R and r are nuclear and electronic coordinates respectively. H is given as

$$H = \sum_{i=1}^{N} \frac{1}{2}\nabla_i^2 - \sum_{i=1}^{N}\sum_{A=1}^{M} \frac{Z_A}{r_{iA}} + \sum_{i=1}^{N}\sum_{j>1}^{N} 1/r_{ij} - \sum_{A=1}^{M} \frac{1}{2M_A}\nabla_A^2$$

$$+ \sum_{A=1}^{M}\sum_{B>A}^{M} \frac{Z_A Z_B}{R_{AB}} \tag{2.2}$$

where M_A= the ratio of mass of nucleus A to the mass of electron;

Z_A = the atomic number of nucleus A;

the first term = the operator for the kinetic energy of the electrons;

the second term = the coulomb attraction between electrons and nuclei;

the third term = the repulsion between electrons;

the fourth term = the operator for the kinetic energy of the nuclei;

the fifth term = the repulsion between nuclei.

Hence, H equals $H_{nuclear}$ +$H_{electronic}$ such that

$$H_{electric} = -\sum_{i=1}^{N} \frac{1}{2} \nabla_i^2 - \sum_{i=1}^{N} \sum_{A=1}^{M} \frac{Z_A}{r_{iA}} + \sum_{i=1}^{N} \sum_{j>1}^{N} 1/r_{ij} \quad (2.3)$$

$$H_{nuclear} = -\sum_{A=1}^{M} \frac{1}{2M_A} \nabla_A^2 + \sum_{A=1}^{M} \sum_{B>A}^{M} \frac{Z_A Z_B}{R_{AB}} \quad (2.4)$$

The problem of solving equation (2.1) with Hamiltonian given in equation (2.2) is a complicated task. To tackle such problem for any practical system needs a lot of approximations. The first well known approximation is Born-Oppenheimer approximation. This approximation helps to eliminate nuclear part and solves Schrodinger equation for $H_{electronic}$ only. The reason behind this is nuclei is heavier than electrons and position of nuclei is considered as fixed hence kinetic energy of nuclei can be neglected and the repulsion between the nuclei can be taken as constant. After solving the problem using $H_{electronic}$, one gets the distribution of electrons which provide the potential in which the nuclei move.

2.2 Hartree Fock Theory

Soon after the discovery of Schrodinger equation in 1926, Hartree introduced a method called self-consistent field method or Hartree method in 1928. Hartree method is the first relatively successful method for finding the wavefunction of the many electron system to calculate the approximate wavefunction and energies for atoms and ions. Later Fock and Slater improved Hartree method by introducing antisymmetry on it in 1930.

Hartree Fock theory is one of the simplest theories for solving many body Hamiltonian. It is based on the approximation that the wavefunction is given by a single slater determinant of N spin orbitals.

$$\Psi = \frac{1}{\sqrt{N!}} \begin{vmatrix} \psi_1(x_1) & \psi_1(x_2) \dots \psi_1(x_N) \\ \psi_2(x_1) & \psi_2(x_2) \dots \psi_2(x_N) \\ & \cdot \\ & \cdot \\ & \cdot \\ \psi_N(x_1) & \psi_N(x_2) \dots \psi_N(x_N) \end{vmatrix} \quad (2.5)$$

where x includes the co-ordinates of space and spin.

The pauli exclusion principle requires that the wavefunction is antisymmetric with respect to change of position of two electrons, that is,

$$\Psi(x_1, x_2, \dots x_i, \dots x_j, \dots x_N) = -\Psi(x_1, x_2, \dots x_j, \dots x_i, \dots x_N) \quad (2.6)$$

Slater determinant meet the requirement of the anti-symmetry principle. Thus no more than one electron can occupy a spin orbital (Pauli exclusion principle). It is convenient to introduce a short hand notation for normalized Slater determinant as given below:

$$\Psi(x1, x2, \dots xN) = |\psi_i(x_1)\ \psi_j(x_2) \dots \psi_k(x_N)> \quad (2.7)$$

Using the wavefunction given in eq.(2.7) in eq.(2.3), an expression for total energy is derived. The variational principle gives the lowest possible energy by varying the single particle wave function

$$E = <\Psi|H|\Psi> \quad (2.8)$$

By minimizing E with respect to choice of spin orbital or varying single particle wave function, the Hartree-Fock equation is derived. The Hartree fock equation is eigenvalue equation of the form

$$f(i)\psi(x_i) = \varepsilon\psi(x_i) \quad (2.9)$$

where f(i) is an effective one electron operator called the Fock operator of the form

$$f(i) = -\frac{1}{2}\nabla_i^2 - \sum_{A=1}^{M}\frac{Z_A}{r_{iA}} + v^{HF}(i) \quad (2.10)$$

where $v^{HF}(i)$ is the average potential experienced by the i^{th} electron due to the presence of the other electrons. The Hartree Fock equation is nonlinear and must be solved iteratively by a self-consistent-field (SCF) method.

The main drawback of Hartree-Fock theory is it does not account for the correlation effects, which leads to an overestimation of electron-electron repulsion in the system, and fail to describe bond breaking or forming [36]. Configuration interaction method is better than Hartree-Fock technique but it is computationally very expensive than Hartree-Fock method as well. The correlation energy E_{corr} is defined from Hartree-Fock energy E_H as

$$E_{corr} = E_{exact} - E_H \tag{2.11}$$

2.3 Density Functional Theory

Density functional theory is presently the most successful approach to compute the electronic structure of material. The original idea of DFT was first introduced by Thomas and Fermi in 1926 which is known as Thomas-Fermi theory and extensions. The idea of the theory is to find the energy of electrons as a function of density. A local approximation based on a free electron model is used to calculate kinetic energy [37]. Thomas-Fermi model is a good approximation for locally homogenous systems but it does not have sufficient accuracy as it failed to predict binding energies and ferromagnetism [38, 39]. Hence this method is of no use for magnetic system. The main reason behind failing of Thomas-Fermi model is due to approximate treatment of the kinetic energy functional [37].

The modern density functional theory starts with the publication of paper by Hohenberg and Kohn in 1964. Introducing two powerful theorems they showed that electron density is the central quantity describing electron interactions in many electron

wavefunction. The first theorem states [40] that the electron density corresponding to many electron ground state wave function determines the external potential V(r) and hence the total energy in which the electron system resides up. In other words, electron density determines the external potential uniquely. Hence, any observable of the system can be written as a functional of ρ(r).

$$\rho(r) = N \int d^3r_1 \dots d^3r_N |\Psi(r_1 \dots r_N)|^2 \delta(r - r_1) \quad (2.12)$$

The second theorem states that the density that minimizes the energy is the exact ground state density.

$$E_0 \leq E_v[\rho] \quad (2.13)$$

where E_0 is the ground state energy, $E_v[\rho]$ is the energy functional of the form

$$E_v[\rho] = T[\rho] + \int d^3r V_{ext}(r)\rho(r) + U_{ee}[\rho] \quad (2.14)$$

where U_{ee} is the electron-electron interaction which can be approximated as

$$U_{ee} = \tfrac{1}{2} \iint d^3r d^3r' \frac{\rho(r)\rho(r')}{|r-r'|} \quad (2.15)$$

Eq.(2.15) is the classical electron-electron interaction given in atomic units of a trial density ρ(r) such that

$$\rho(r) \geq 0 \; and \; \int \rho(r) d^3(r) = N \quad (2.16)$$

$T[\rho]$ and $U_{ee}[\rho]$ are universal functional, which means they are the same for all electronic systems but the second term in eq.(2.14) is system dependent. The ground state energy is get by minimizing the energy functional in eq.(2.14). Still there are two main problems: the exact form of the kinetic energy functional is not known, and the electron-electron term is approximated by considering classical electron densities. Electron-electron interaction should also depend upon correlations of each electrons position and should follow Pauli principle.

To fix such issues, Kohn and Sham in 1965 proposed a new approach [33]. They wrote the energy functional as [30]

$$E[\rho] = T_0[\rho] + \int \left[V_{ext}(r) + \frac{1}{2}\phi(r)\right]\rho(r)dr + E_{xc}[\rho] \quad (2.17)$$

where $T_0[\rho]$ is the kinetic energy functional of non-interacting electron system, $V_{ext}(r)$ is the external potential energy due to nuclei, $\phi(r)$ is the classical coulomb potential for electrons, and $E_{xc}[\rho]$ the exchange-correlation energy. E_{xc} includes correction to $T_0[\rho]$ and also non-classical terms of electron-electron interaction.

By minimizing the energy functional with respect to the density we get the definition of chemical potential in DFT

$$\mu = \frac{\delta E[\rho(r)]}{\delta\rho(r)} \quad (2.18)$$

substituting (2.17) into (2.18) one gets

$$\mu = \frac{\delta T_0[\rho(r)]}{\delta\rho(r)} + V_{eff}(r) \quad (2.19)$$

V_{eff} in eq.(2.19) is Kohn-Sham effective potential which is defined as

$$V_{eff}(r) = V_{ext}(r) + \frac{\delta E_{xc}(\rho)}{\delta\rho(r)} + \phi(r) \quad (2.20)$$

Now to get electron density that satisfies eq.(2.19), we solve the following N one-electron equations [33]

$$\left[-\frac{1}{2}\nabla^2 + V_{eff}(r)\right]\Psi_i = \varepsilon_i\Psi_i \quad (2.21a)$$

or $$\left[-\frac{1}{2}\nabla^2 + V_{ext}(r) + \frac{\delta E_{xc}(\rho)}{\delta\rho(r)} + \phi(r)\right]\Psi_i = \varepsilon_i\Psi_i \quad (2.21b)$$

And

$$\rho(r) = \sum_i^N |\Psi_i(r)|^2 \quad (2.22)$$

By making an initial guess for ρ(r), V_{eff} is calculated using eq.(2.20) and then again using (2.21) and (2.22) new ρ(r) is calculated. Hence, self-consistent method is

implied to find V_{eff} and ρ(r). Once we get consistent results, the total energy is calculated by using eq.(2.17) where T_0 is given as

$$T_0[\rho] = \frac{1}{2}\sum_{i=1}^{N} < \Psi_i|\nabla_i^2|\Psi_i > \quad (2.23)$$

The main significance of Kohn-Sham scheme is only E_{xc} is approximated and all other contribution to the total energy functional are treated exactly.

2.4 The Exchange Correlation

2.4.1 Local Density Approximation (LDA)

LDA is an approximation to exchange-correlation (XC) energy functional that depends upon the value of electronic density at each point in space. One of the way to get a successful approximation is to derive it from the homogenous electron gas [36]. Within this approximation the exchange-correlation energy is written as

$$E_{xc}[\rho] = \int \rho(r)\varepsilon_{xc}[\rho(r)]dr \quad (2.24)$$

The exchange-correlation energy is divided into exchange and correlation terms as shown

$$E_{xc} = E_x + E_c \quad (2.25)$$

where E_x is the exchange energy and E_c is the correlation energy.

The exchange term takes on a simple analytic form for the homogenous electron gas whereas the correlation terms can lead to a different approximations as shown by different literature [40 – 42]. LDA works well for ground state geometries, vibration and phonon calculations but it usually underestimates band gap of semiconducting materials and also lattice constants.

2.4.2 Generalized Gradient Approximation

GGA is the first logical step to go beyond LDA. In this approximation, we not only use the information of ρ(r) at a particular point r but also consider the density of gradient of charge density, ∇ρ(r), in order to include non-homogeneity of the true electron density. Thus, we can write exchange-correlation energy in GGA in the following form

$$E_{xc}^{GGA}[\rho_\alpha, \rho_\beta] = \int f(\rho_\alpha, \rho_\beta, \nabla\rho_\alpha, \nabla\rho_\beta)dr \quad (2.26)$$

There are many function proposed; PW91 and PBE are some of the common ones. There are many advantages of GGA over LDA [43-47]. Few significance of GGA's are improve ground state properties and improvement in lattice parameters.

2.5 DFT+U

Although DFT gives a lot of good structural properties, such as lattice constant, phonon spectrum, formation energies, and also electronic properties, such as ionization potentials, excitation energies, it has certain drawbacks as well. It has been observed that both LDA and GGA cannot predict the behavior of highly localized d and f states accurately [48]. For many transition metallic compounds, DFT underestimates the band gap significantly. Such discrepancy arises in calculation due to improper treatment of the self-interaction correction (SIC) of the electrons [49]. This can be improved by following Anderson model [50] where Hilbert space is divided into two subsystems: i) d and f orbital- for which more orbital dependent coulomb interaction is required; and ii) s and p orbital which are treated well by LDA and GGA. To correct the electronic interaction of localized orbital electron, U parameter, known as Hubbard parameter, is added in LDA or GGA calculation. The Hubbard parameter U is defined as

$$U = E(d^n + 1) + E(d^n - 1) - 2E(d^n) \quad (2.27)$$

Eq.(2.27) simply denotes coulomb energy cost in order to put two electrons at the same place. The new energy functional then is given as

$$E^{(DFT+U)} = E^{DFT} + E^{U}[\rho_m^{I\sigma}] - E^{dc}[\rho^{I\sigma}] \quad (2.28)$$

where E^{DFT} is standard DFT functional, $E^{U}[\rho_m^{I\sigma}]$ is Hubbard correction term, and $E^{dc}[\rho^{I\sigma}]$ is called the double counting term which is used to avoid the double counting of energy contribution of these orbitals included in $E^{U}[\rho_m^{I\sigma}]$. DFT+U functional in above equation only include the onsite coulomb repulsion but neglect the proper treatment of exchange interaction. Such improper treatment can be improved by redefining the U parameter as U^{eff}

$$U^{eff} = U - J, \quad (2.29)$$

where J is Stoner exchange parameter. Using both onsite coloumb interaction and exchange interactions , the total energy functional of DFT+U is then written as

$$E^{(DFT+U)} = E^{DFT} + E^{U}[\rho_{mm'}^{I\sigma}] \quad (2.30)$$

where $E^{U}[\rho_{mm'}^{I\sigma}]$ is the simplified form of the Hubbard correction to the energy functional [51, 52] which correct the known deficiency of LDA and GGA of underestimating the localization in highly localized orbitals.

$$E^{U}[\rho_{mm'}^{I\sigma}] = E^{U}[\rho_m^{I\sigma}] + E^{dc}[\rho^{I\sigma}] \quad (2.31)$$

$$= \frac{U^I}{2}\sum_{i,\sigma}\sum_i \lambda_i^{I\sigma}(1-\lambda_i^{I\sigma}) \quad (2.32)$$

with $0 \leq \lambda_i^{I\sigma} \leq 1$ and U^I is the coulomb repulsion parameter on atomic site *I*.

2.6 Hybrid Method

This method of approximation incorporates exact exchange from Hartree Fock with exchange-correlation term from LDA or GGA. Hybrid functionals are better than DFT in determining band gap, vibrational properties, static and dynamic dielectric function and

also magnetic properties. Hybrid functional are step forward compared to LDA and GGA but still it is not a universal improvement and not as cost effective as standard DFT calculation.

There are many hybrid functional in use such as B3LYP, HSE, and MO6. In our study we use HSE06 [53 – 55] functional.

$$E_{XC}^{HSE} = \alpha E_X^{SR}(\mu) + (1-\alpha)E_X^{PBE,SR}(\mu) + E_X^{PBE,LR}(\mu) + E_C^{PBE} \quad (2.33)$$

where E_C^{PBE} is the PBE functional for the correlation energy, SR and LR denotes short range and long range part of the electron-electron interaction respectively. The mixing coefficient α was set to ¼ i.e only 25% of exact exchange was used in the present work. For screening parameter, μ = 0.2 $Å^{-1}$ was used as required in HSE06 functional.

2.7 Computational Details

All the calculations were performed within the framework of the standard projector augmented wave method using DFT as implemented in Vienna ab initio simulation package (VASP) [56, 57]. The Projected Augmented Wave (PAW) method [58] is an effective method used in ab initio calculation as it is a generalization of pseudopotential and augmented plane wave method. The PAW method transforms rapidly oscillating wavefunctions into smooth wavefunctions making it computationally convenient and making it effective to calculate all-electron properties from these smooth wavefunctions. PAW is an all-electron like method and hence does not require non-linear core correction. Generealized gradient approximation was used to treat exchange and correlation potential as parameterized by Perdew-Burke-Ernerhof (PBE) [43, 59]. PBE functional works better on a wide range of elements because it does not contain any empirically optimized parameters. Understanding the failure of DFT in predicting band structure and treating localized d and f orbitals, we employ an on-site Coulomb

correlation parameter called U parameter or Hubbard like parameter in some of our calculation. In the absence of excess theoretical and empirical data of Cu_2S, choosing an appropriate U value is quite difficult for DFT+U calculation. Therefore special care was taken while performing DFT+U calculation by providing different U on Cu-d in lowest energy structure from DFT. Then properly analyzing and comparing electronic structure, mainly band structure, with DFT and DFT-hybrid results, we choose U = 7 as an approximate U value for our calculation. Inorder to compensate extra magnetic effect caused by U parameter, stoner exchange parameter or j parameter was also used. The value of j used was 1 eV. For ionic relaxation, each ion was relaxed until the force on it is equal or less than 0.01eV/Å and 400 eV was used for the energy cut off for the plane wave basis set. Density of States (DOS) plots were generated using tetrahedron method using different meshes depending upon unit cell size.

We also studied Cu vacancy structure and calculated defect formation energy using DFT. The defect formation energy of Cu vacancies was obtained using the following equation

$$E_f = E_{tot}(D) - E_{tot}(0) + n\mu_{cu} \quad (2.34)$$

where $E_{tot}(D)$ is total energy of Cu-vacancy cell, $E_{tot}(0)$ is total energy of cell without vacancy, n is the number of Cu atoms removed from a defect free cell and μ_{cu} is the chemical potential of Cu. In order to understand the stability issue of these structures, we calculated the heat of formation of Cu_xS using the definition

$$\Delta H = E(Cu_xS) - xE(Cu) - E(S) \quad (2.35)$$

where ΔH is heat of formation, $E(Cu_xS)$ is the total energy of primitive cell, E(Cu) and E(S) are total energy per Cu atom in bulk phase and per S atom in stable S_8 phase respectively. A DFT study is also done on tin doped Cu_2S and oxygen doped Cu_2S. A software program called VESTA [60] was used for visualization purposes.

Chapter 3

Stiochiometric Copper Sulfide (Cu_2S)

3.1 Determining Lowest Energy Structure

In the lack of proper theoretical description of the structure, we initialize our study by collecting information about numerous possible Cu_2S structure from various sources; we not only include structures published in experimental literatures [17, 18] but also consider other new possible structures as well. The trail structures were selected in the following way: Material project website [61] provides lattice parameters and initial co-ordinates for ten structures (structures with only number assigned to them in table 1). Some structures were selected from similar sulfide and copper structures respectively: acanthite like and berzeanilite like structures are similar to acanthite (Ag_2S) and berzelianite (Cu_2Se) where Ag is replaced by Cu and Se is replaced by S respectively. The reason behind choosing Ag_2S is Ag falls directly below Cu in periodic table and they have similarity in their electronic structures. Similarly Se lies below S in periodic table. AF denotes antiflourite structure. The information for remaining structures is acquired from previously published literatures on Cu_2S [17, 18, 23, 24].

After collecting information about all the possible structures, the structures were relaxed fully within the framework density functional theory. Table 3-1 shows the cohesive energy for all the different structures per formula unit. From table 3-1, we see that acanthite like structure is energetically favorable among all structures, followed by str2, low chalcocite and str4. The cohesive energy of acanthite like structure is -10.653 eV per formula unit. The structures are arranged in the order of their stability in figure 2-1 with relative energy given below each structure as compared with lowest energy structure. Figure 3-1 clearly shows that acanthite like is more favorable than low

chalcocite by 16 meV and interestingly acanthite like, str2 and low chalcocite all are monoclinic in nature as well. As DFT usually underestimate localization in d-orbital we also performed DFT+U calculation on selected structures to check the validity of DFT. The outcome of DFT+U is presented in table 3-2. DFT+U authenticates DFT prediction consenting that acanthite like structure is the most energetically favorable structure at 0 K theoretically. Hence acanthite like is the ground state structure of Cu_2S. The difference in energies between low chalcocite and acanthite like structures is 57 meV at DFT+U level of theory. In table 3-3 we present fully optimized DFT lattice parameters for lowest energy structures. It is noticed in table 3-3 that almost all the lattice angle are 90^0 in acanthite like. Low chalcocite has larger lattice constants because unit cell of low chalcocite contains significantly more atoms than any other unit cell structure. This will be discussed later in this chapter.

Table 3-1 Cohesive energy for probable structures for Cu_2S using DFT.

Structure	**Cohesive energy per formula unit (eV)**
Str1 (Acanthite like)	-10.653
Str2	-10.638
Str3 (Low chalcocite)	-10.637
Str4	-10.629
Str5	-10.503
Str6	-10.436
Str7	-10.427
Str8 (AF)	-10.379
Str9	-10.347
Str10 (Berzelianite like)	-9.995
Str11	-9.971
Str12 (Hexagonal)	-9.943
Str13	-9.988
Str14	-9.881
Str15	-9.854

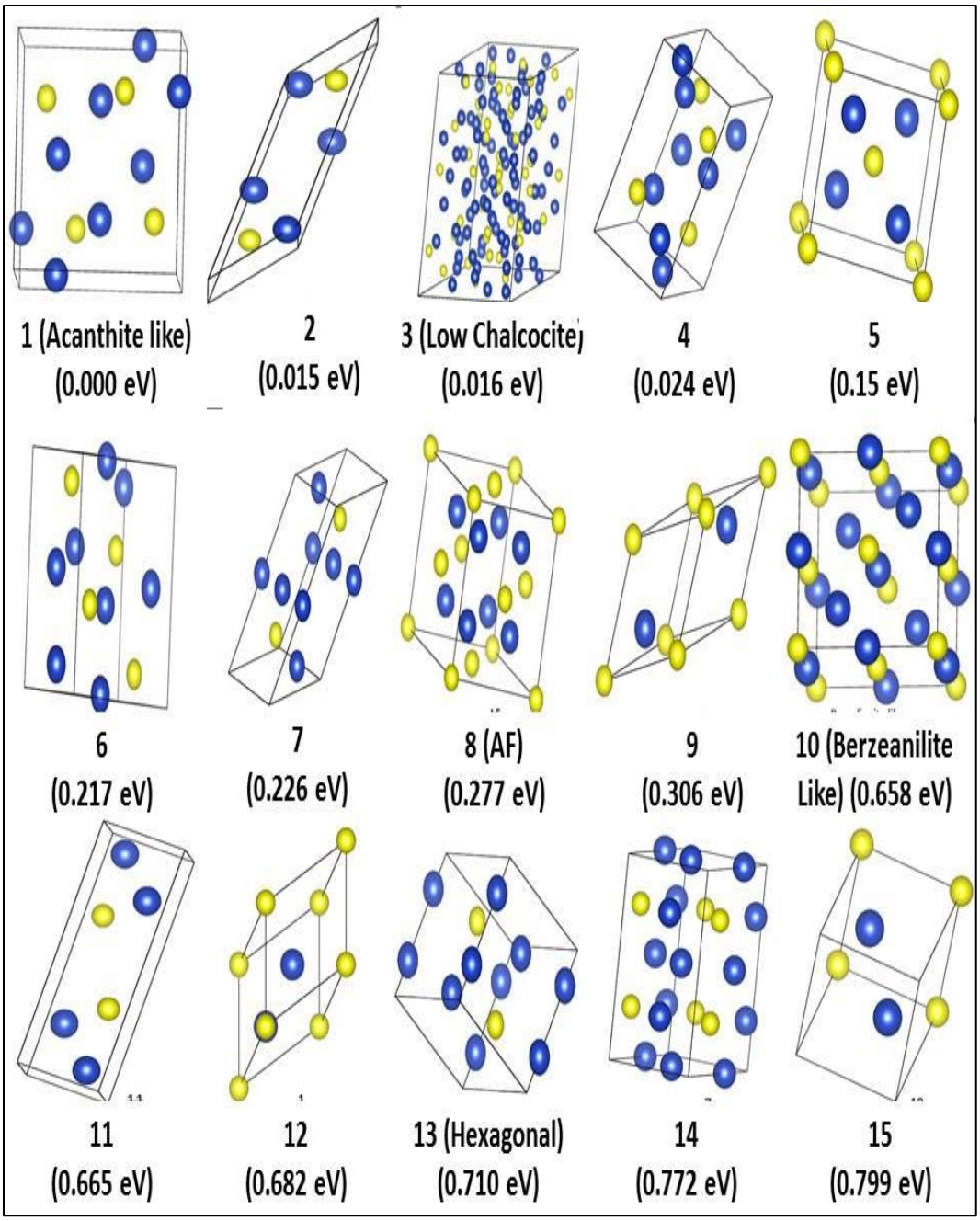

Figure 3-1 All probable structures with relative DFT cohesive energy per formula unit as compared with lowest energy structure energy.

Table 3-2 Cohesive energy for some of the selected structure calculated using DFT+U=7.

Structure	**Cohesive energy (eV) per formula unit using DFT+U**
Acanthite like	-5.466
Str2	-5.422
Str4	-5.427
Low chalcocite	-5.409

Table 3-3 Lattice parameters and average copper-copper bond length of selected Cu_2S structures using DFT.

Structure	**Lattice Parameter**						**Cu-Cu layer**	**Average Cu-Cu bond (Å)**
	a (Å)	**b (Å)**	**c (Å)**	**α (˚)**	**β (˚)**	**γ (˚)**		
Acanthite like	4.00	7.16	6.88	90.0	89.29	90.0	Yes	2.67
Str2	3.93	5.13	8.45	90.0	144.3	90.0	Yes	2.61
Low Chalcocite	15.07	11.94	13.32	90.0	116.1	90.0	No	2.65
4	4.01	6.52	7.03	90.0	90.0	90.0	No	2.71

3.2 Structural Differences Between Acanthite Like and Low Chalcocite

The above results create a discrepancy between our theoretical results, and experimental results. From our results one can see that minimum energy structure corresponds to acanthite like but not the suggested experimental low chalcocite structure. Hence, it is important to have a good understanding of fundamental differences between these two structures. The two structures are presented in figure 2. Low chalcocite is monoclinic in nature containing 96 Cu atoms and 48 S atoms per unit cell. Acanthite like is also monoclinic in nature with 8 Cu atoms and 4 S atoms per unit cell. The volume of unit cell of low chalcocite is almost 11 times more than that of acanthite like whereas average volume per formula unit in acanthite like is greater by 4.51 $Å^3$ as compared with low chalcocite. Besides having differences in lattice parameters and cell structure as provided in table 3-3, it is clearly visible in figure 3-2 that a stark difference between the two structures is the arrangement of Cu atoms. Cu atoms are well organized in acanthite like forming two dimensional layers. Similar kind of layer is also observed in str2, as shown in figure 3-3, which suggests that arrangement of Cu may play a role in energy minimization.

Interestingly at DFT+U level, str2 is 13 meV formula unit lower in energy than the low chalcocite structure and acanthite like is 44 meV more stable than str2. Therefore, it seems that the presence of Cu layer with comparatively more space for each atoms make acanthite like energetically more favorable than low chalcocite. In these layers average Cu-Cu bond length in most of the lower energy structures calculated using DFT is in the range between 2.61 Å – 2.71 Å with 2.67 Å for acanthite like as provided in table 3-3. Average Cu-Cu bond length is only 3.5-4% higher than metallic Cu-Cu bond length which is 2.55Å (DFT). In most of Cu compounds, like Cu_2O, average Cu-Cu distance is

more than 3.00 Å [62]. This low Cu-Cu distance in Cu_2S compared to metallic Cu indicates high Cu-Cu interactions.

Acanthite like structure is interestingly very simple which contains only one kind of copper atoms and copper atoms are arranged in layers with Cu-Cu distances greater than or equal to 2.67 Å with Cu-S bond length 2.31 Å and average S-Cu-S angle is about 120^0. Similar kind of arrangement for Cu_2S was also observed in one of study conducted by Janosi in 1964 at about 2kbar pressure [63].

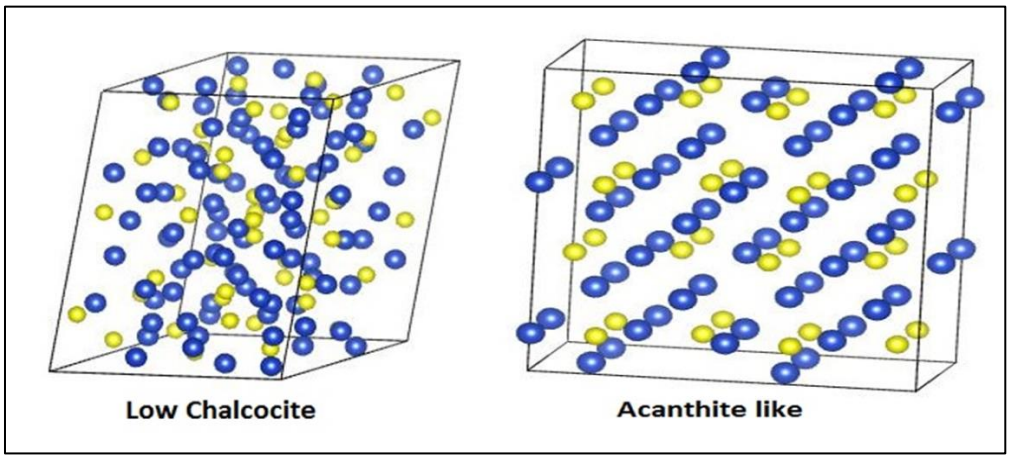

Figure 3-2 Structure for experimentally favorable (low chalcocite) and theoretically determined (acanthite like) structures. Blue color denotes Cu atoms and yellow color denotes Sulfur atoms.

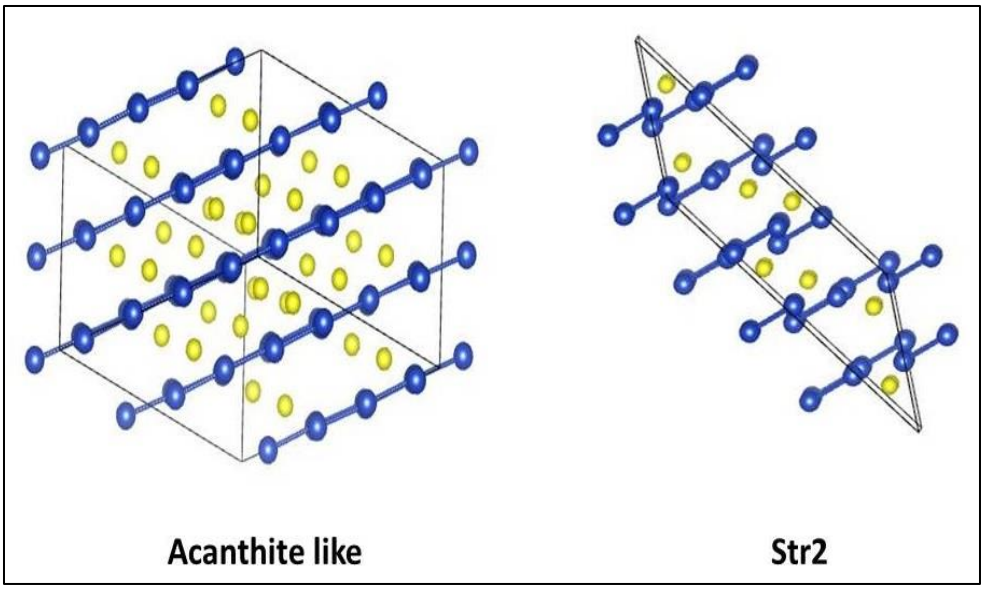

Figure 3-3 Acanthite like and str2 structures showing presence of Cu layers. Blue atom is copper and yellow atom is sulfur.

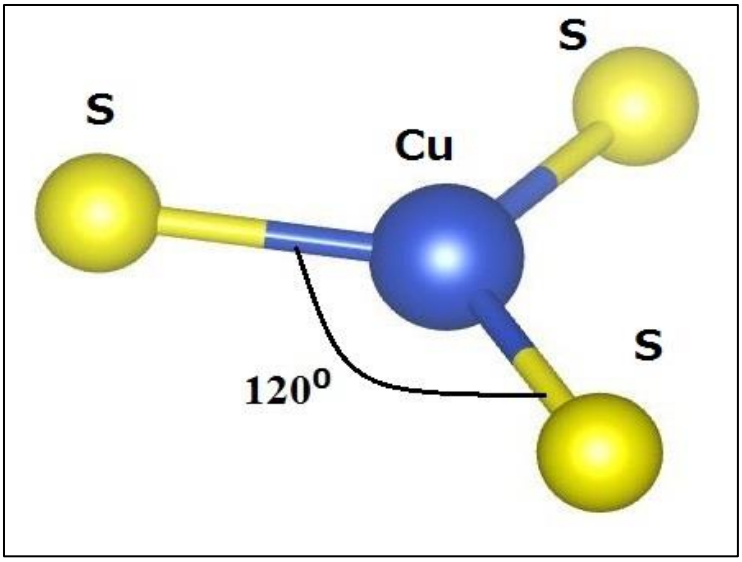

Figure 3-4 S-Cu-S bond angle in acanthite like structure.

3.3 Electronic Properties

3.3.1 A brief comparison of dos of low chalcocite and acanthite like

Electronic property is another important criterion to understand in material to fully optimize its potential. We compare partial density of states for low chalcocite and acanthite like calculated using DFT in figure 3-5. It is clear that partial dos of those materials are almost similar. We see prominent peak between -15.6 eV to -13.5 eV (DFT) corresponding to S-s, and also peaks around -6 eV are due to Cu-d and S-p in both cases. There is a gap between -14 to -7.5 eV in dosplot corresponding to no band state in both pdos. The top of the valence band is dominated by Cu-d in Cu_2S which is a common characteristic of many other chalcogenide PV materials like CZTS, $CuInS_2$, $CuGaS_2$, $CuInSe_2$ [64, 65]. There is not much difference in conduction band between two structures as well. It is interesting that a conduction band minimum (CBM) is composed of Cu-p in both pdos. The bands above CBM are formed due to hybridization of Cu-d and S-p. Although structurally they are different, their electronic structure is similar in nature. As acanthite like does not have complex structure like low chalcocite, use of acanthite like structure in theoretical study is computationally easier and less expensive. Acanthite like structure can eliminate the barrier we are having so far in understanding the properties of Cu_2S.

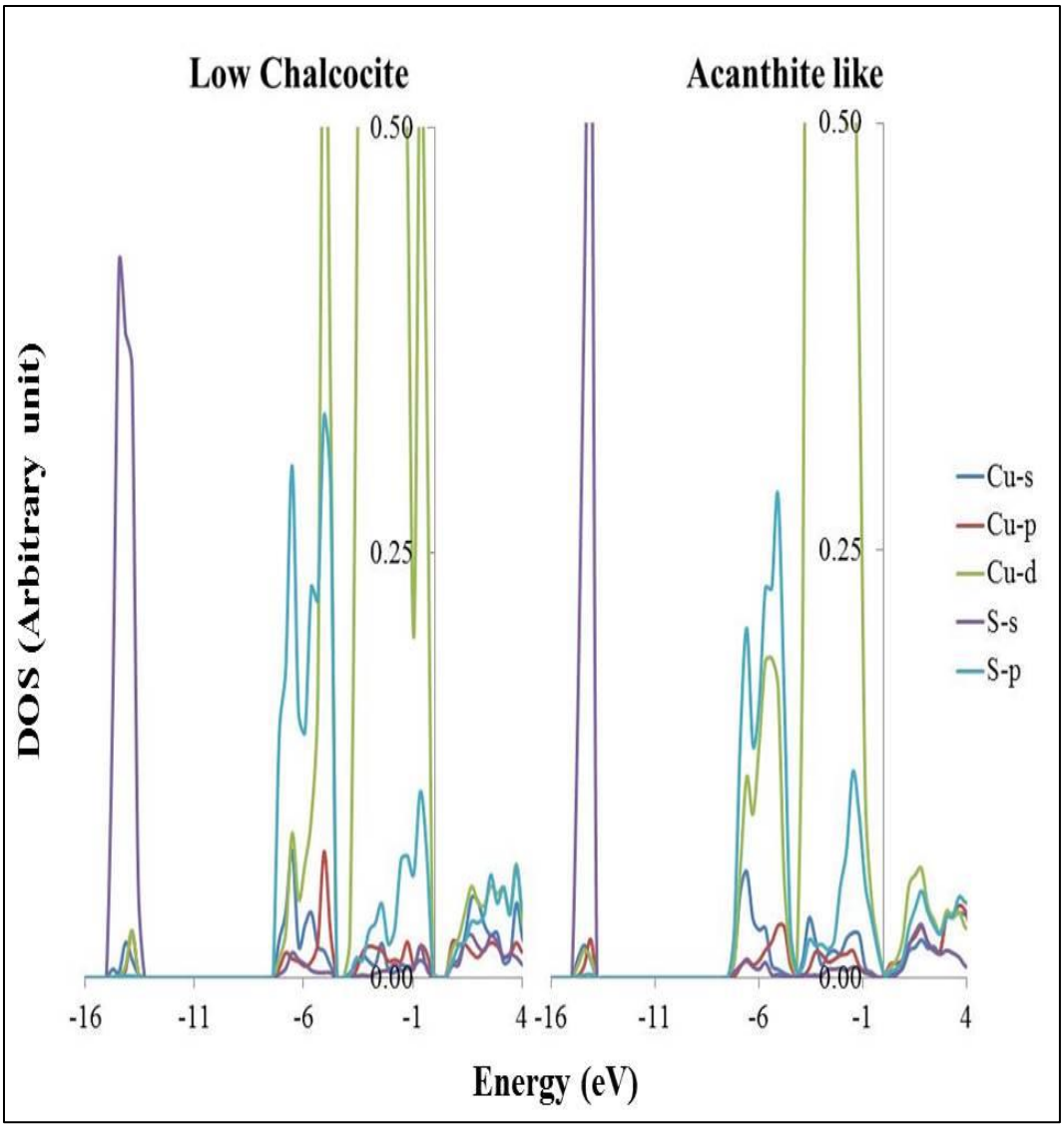

Figure 3-5 Partial dosplots from DFT calculation. The left one represents pdos of low chalcocite and the right one is for acanthite like structure.

3.3.2 Electronic structure of acanthite like

Now we mainly focus on acanthite like structure as it is theoretically determined lowest energy structure with well-defined Cu positions which makes the study of Cu_2S

easier and simpler. Understanding the shortcoming of DFT, mainly in determining band structure, we also performed DFT+U and DFT-hybrid calculations. As expected DFT underestimate the band gap which can be seen in figure 3-6; there is overlap of valence band maxima (VBM) and conduction band minima (CBM) creating a negative band gap. The band gap widens with the use of U on Cu-d and hybrid DFT calculations as compared with regular DFT result. We find a band gap of 0.694 eV for U = 7 whereas for Hybrid it is 0.609 eV with 25% exact exchange, compared to the experimental gap of 1.21 eV [25]. The band gap is indirect in both DFT+U and DFT hybrid calculation located along Γ→Y. The overall features of band structure of DFT+U and DFT-Hybrid remain the same as DFT-GGA calculation with slight changes in the nature of conduction band with DFT+U and also in Hybrid calculations- it is clearly visible that at Γ point the concave nature of CBM has changed becoming more flat in case of U= 7 affecting the effective mass of electron. In the vicinity of Γ point the conduction bands are less dispersive indicating higher effective electron mass. However, conduction bands are more dispersive around other symmetry points. The band gap in hybrid calculation can be further increased by increasing the exact exchange contribution but we will leave this band gap issue later for future work as it is not a primary focus of our current work. From figure 3-7, it can be inferred that there is a downward shift in valence bands with the increase in U values. This downward shift of valence bands with U on Cu-d means localization signifying Cu-d dominates valence bands near fermi level. Increasing value of U does not only shift the occupied band in downward direction but also shift the conduction band upward which results in increase in optical transition energy between valence and conduction band states. Hence, band gap increases.

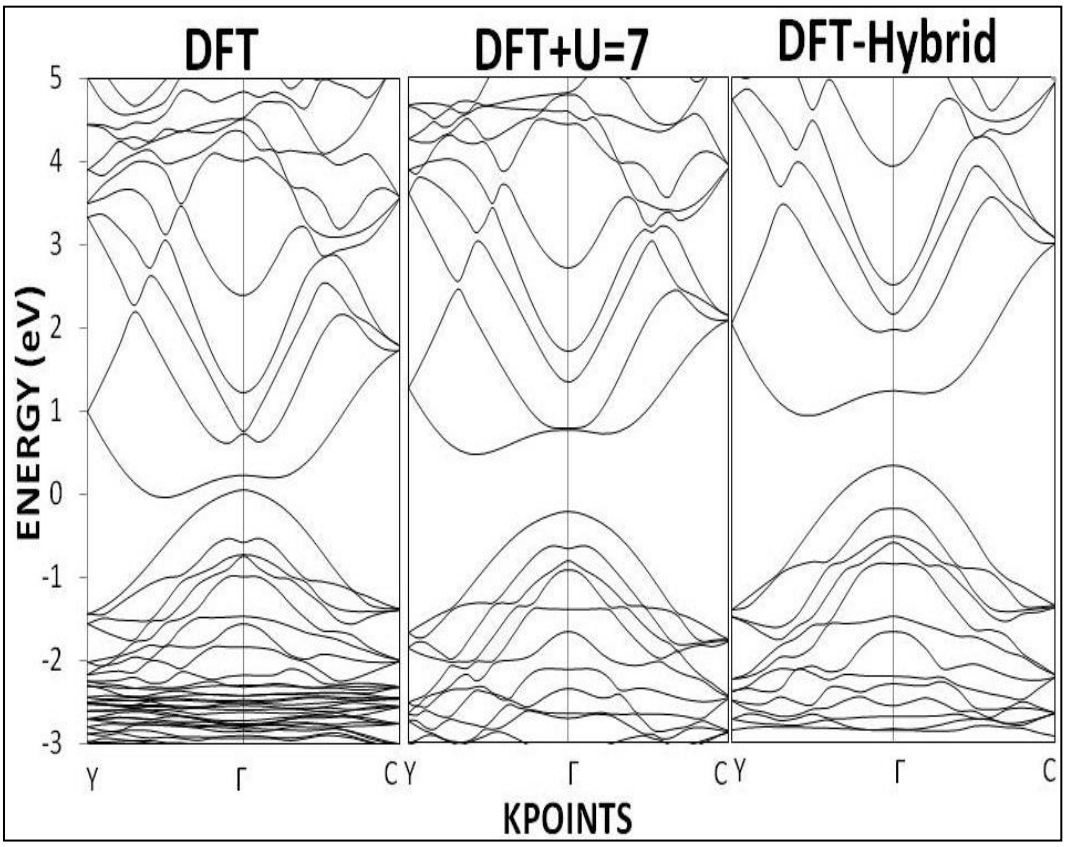

Figure 3-6 Band Structures for acanthite like structure. The first one on the left is for DFT calculation, the middle one is for DFT with U = 7 on Cu-d and the last one on the right is for DFT-hybrid.

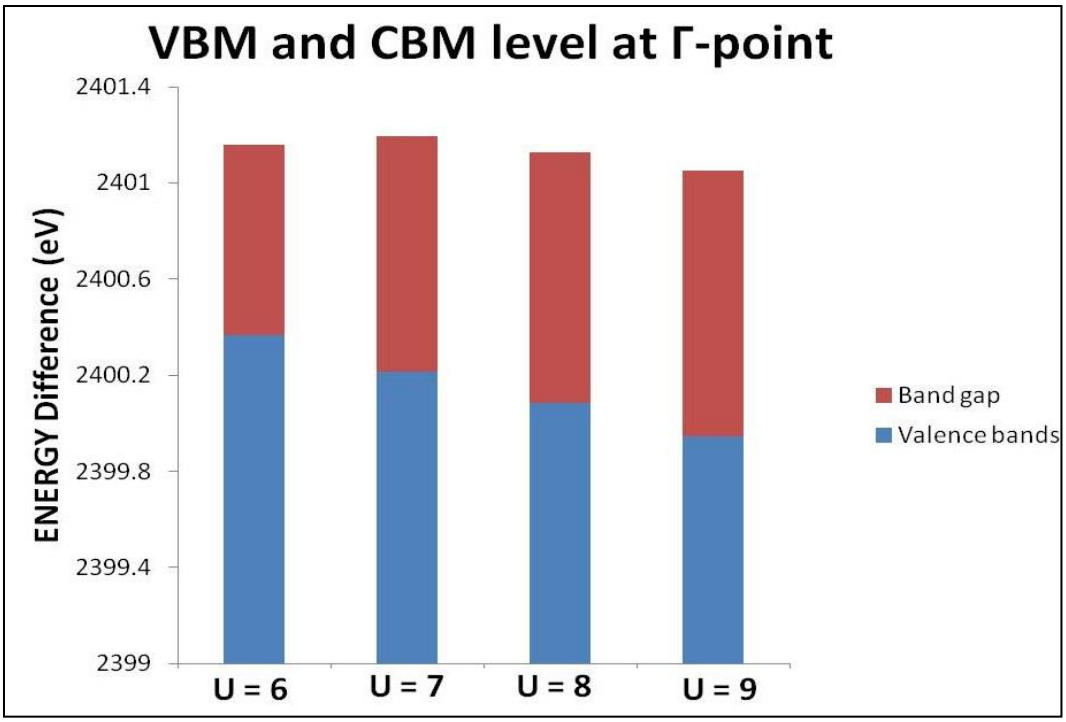

Figure 3-7 Valence band and conduction band level for acanthite like structure at gamma-point as compared with the energy value of innermost S-1s level. The top most part in the figure is CBM level at gamma point. U below each bar represents different U values used in calculation.

The band gap opening with U is also visible in total dos (figure 3-8). Figures 3-9 and 3-10 present the partial dos obtained from DFT and DFT+U for acanthite like. Pdos plots show that contribution to the region at the top of valence band comes from Cu-d and S-p but it is also clearly visible from pdos plots that Cu-d orbital dominates the valence band as discussed above. Contribution from any other orbital is very minimal around valence band whereas around the core level S-s is more prominent. Conduction bands seem to be formed due the hybridization of Cu-d and S-p orbital's with slightly greater contribution from the former and the peak around 1.6 eV look flatter in case of U

= 7. One of the reasons for an increase in band gap with the use of U is due to a decrease in the hybridization level (less contribution from Cu-d) at conduction bands which is also somewhat visible in charge density plots as shown in figure 3-11. Hybrid and DFT+U charge density plots show decrease in charge density as neck narrows down. Figure 3-11 also displays the fact that the bonds become more ionic with DFT+U and DFT hybrid. As ionic bonds are weaker than covalent bonds this can aid in breaking bonds and forming vacancies.

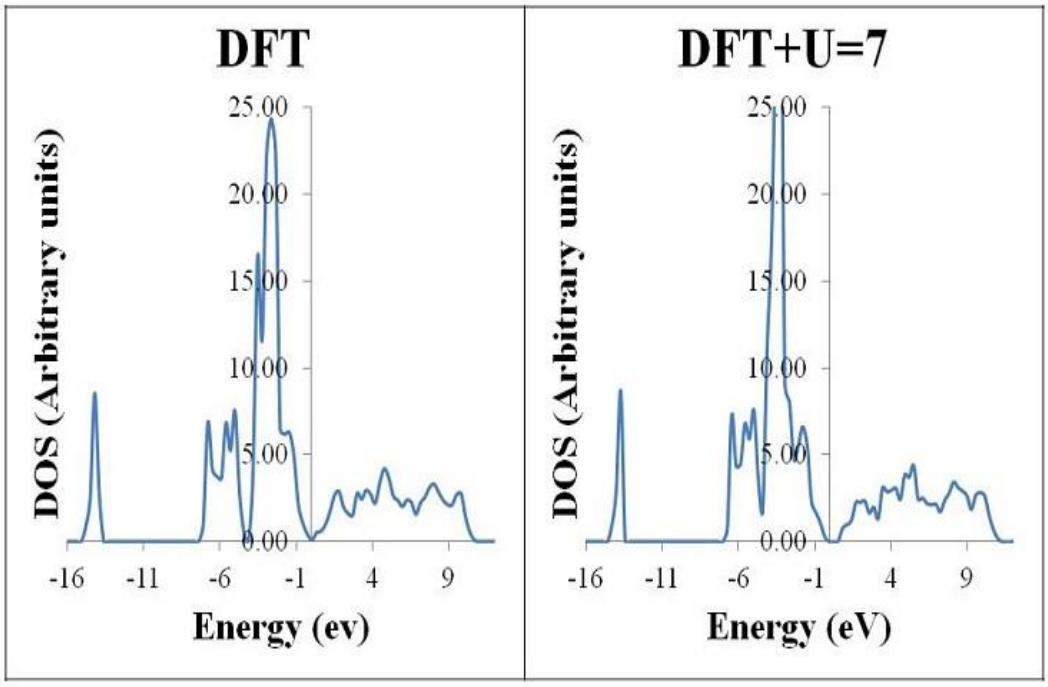

Fig 3-8 Total dosplots for acanthite like structure. The left figure is for DFT calculation whereas right one is for DFT+U = 7 at Cu-d.

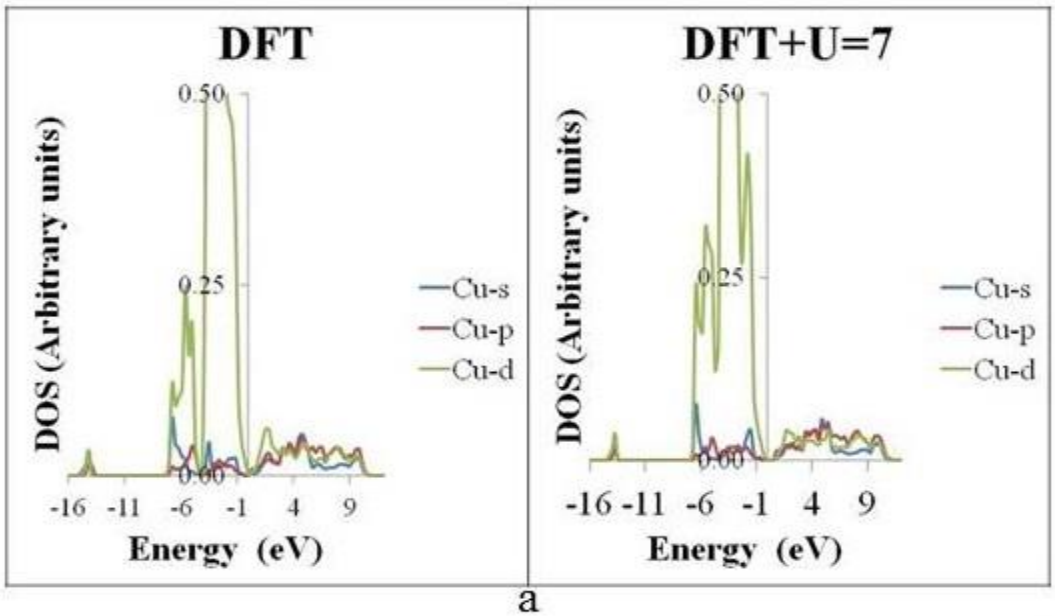

a

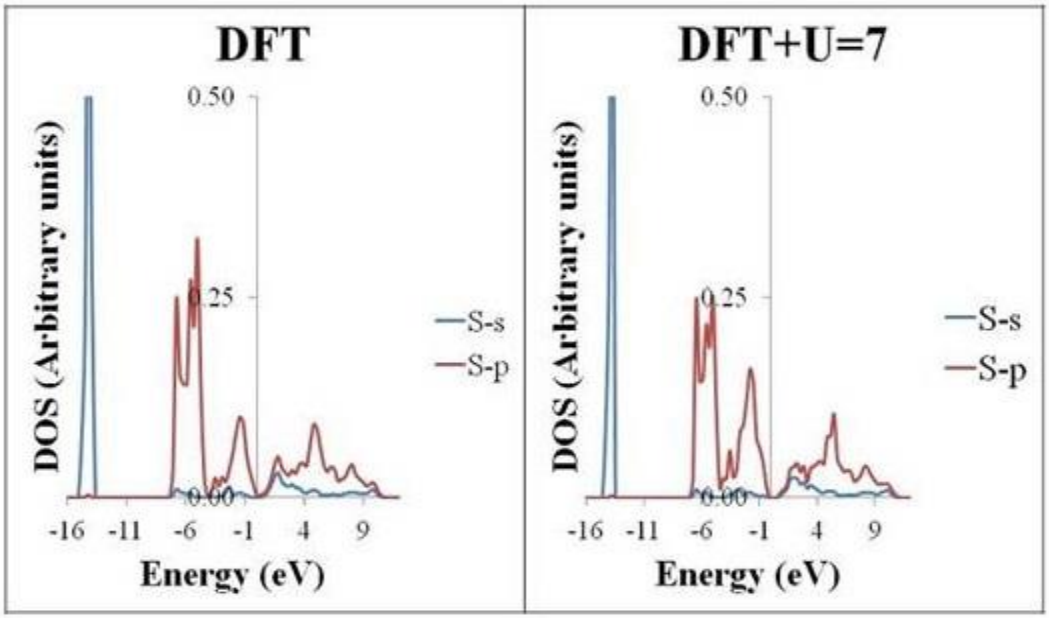

b

Fig 3-9 Partial dosplots for acanthite like structure. The left figure is for DFT calculation and the right one is for DFT+U = 7 on Cu-d.

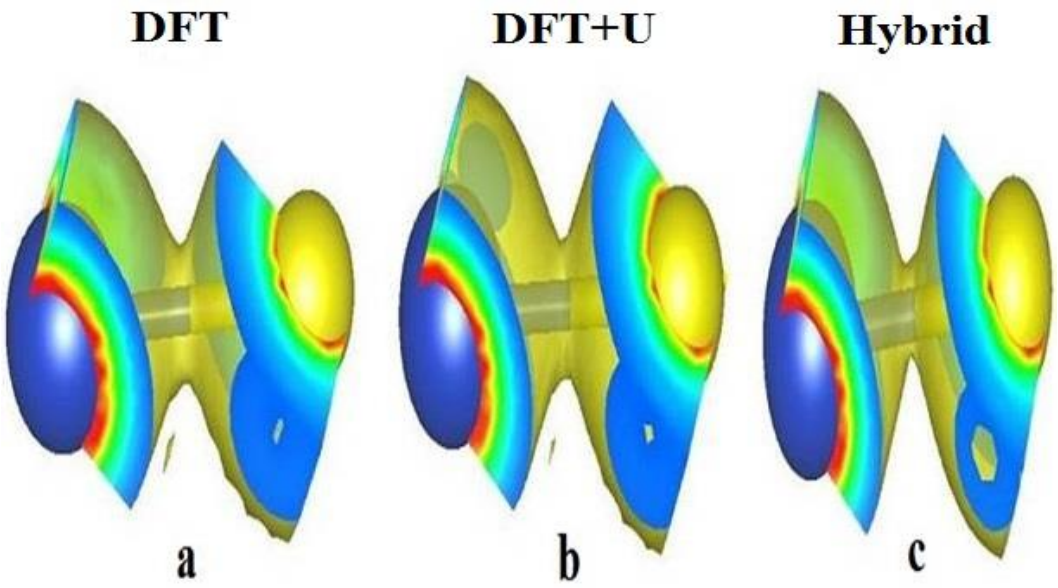

Fig 3-10 Electron charge density for acanthite like structure calculated by using three different methods. (a) Using DFT, (b) using U = 7 on Cu-d, and (c) using hybrid DFT.

3.4 Cu-Cu Bonding in Acanthite Like

As discussed above average Cu-Cu bond distance in Cu_2S is just about 3.5-5% of metallic Cu-Cu distance whereas for other materials like Cu_2O it is comparatively larger. This small Cu-Cu distance opens up an interesting question- about what will happen to the structure if the bond distance is decreased further between copper atoms?

In order to solve above mentioned problems, we created a 2x2x2 supercell of acanthite like structure by forming atleast three Cu-Cu bonds among Cu's in one of the layers with bond length less than metallic copper. Our calculated metallic bond length of copper of 2.55Å is in good agreement with other's caculations- 2.448 Å [66], 2.556 Å [67]. This supercell, with some Cu-Cu bond length less than metallic copper, was fully relaxed and then the bond length was calculated again. Cu_2S does not favor bonding between two Cu atoms with value less than metallic Cu bond length as copper atoms go back to

their original position. To reach to a proper conclusion about bonding between Cu atoms and stability, the bonds were also created between Cu atoms of different layers and similar calculation was done. After full relaxation, Cu atoms are no longer arranged in layers as shown in figure 3-12 but the total energy seems to increase by 0.11 eV per formula unit. A stable structure cannot be formed with bonding between Cu atoms of different layers. This directly indicates that it is highly unlikely that Cu atoms stay close and hence they tend to repel each other trying to stay farther. Overall, it can be concluded that Cu_2S doesn't prefer Cu-Cu bonding below 2.55Å. There is a repelling behavior of Cu in Cu_2S which could aid up in the formation of Cu vacancy.

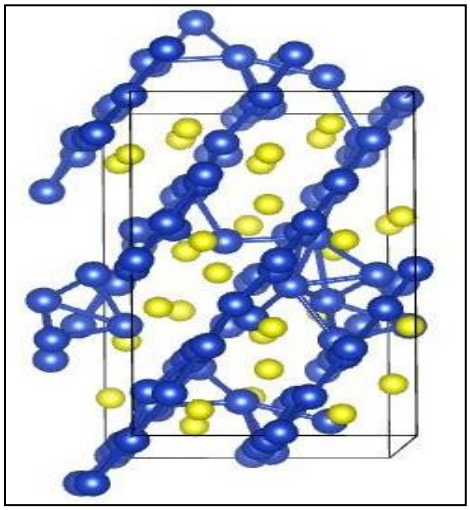

Fig 3-11 Acanthite like structure with bonding between Cu of different layers.

Chapter 4

Study of Copper Vacancy in Cu_2S

4.1 Introduction

Copper sulfide (Cu_2S) is not a stable compound as said before as it suffered a deterioration in air and as a result it forms copper vacancy. Most of the copper sulfides that exists are in the form Cu_xS where $x < 2$. Some of the commonly known copper sulfides with $x < 2$ are: djurleite ($Cu_{1.94}S$), digenite ($Cu_{1.80}S$) and anilite ($Cu_{1.75}S$). The use of Cu_2S in solar cell gave around 9% efficiency in the past but its efficiency decreases with time. High copper vacancy makes a material high p-type which ultimately makes the structure more unstable and could not conduct electrons properly. It is necessary to make a proper study on copper vacancy in Cu_2S. We are mainly going to focus on Cu-vacant acanthite like structure with brief discussion on other structures as well.

4.2 Vacancy Formation in Acanthite Like

4.2.1 Formation energy

Acanthite like structure has 8 Cu atoms and 4 Sulfur atoms. In order to create a Cu-vacancy in Acanthite like, we created a supercell of acanthite like. First of all Cu to S ratio of 1.97 was created. The structure was then relaxed fully using DFT. The heat of formation of $Cu_{1.97}S$ (acanthite like) is -0.447 eV, however it is only -0.435 eV for Cu_2S (without vacancy). The difference of 12 meV energy suggests that acanthite like structure also shows a tendency of forming Cu vacancy as suggested for Cu_2S. In order to know more about vacancy forming trend, we further created vacancy on acanthite like structure. The lowest Cu to S ratio created was 1.75 as previous literatures [23, 24] have mentioned that Anilite ($Cu_{1.75}S$) is the most stable copper vacant structure. Heat of

formation tells us about the stability of the material but to know about the probability of forming such acanthite like based vacant structure, we also calculated defect formation energy at two extreme cases. The result of defect formation energy calculation is provided in table 4-1, at both Cu-rich and Cu-poor condition for different vacancies. To visualize the results more clearly, a defect formation energy behavior per copper vacancy with respect to copper chemical potential is drawn in figure 4-1 for different copper vacant structures. At Cu rich and Cu poor limit, the defect formation energies for $Cu_{1.97}S$ are -0.367 eV and -0.585 eV respectively. Figure 4-1 clearly shows defect formation energy increases with increasing vacancies and for Cu to S ratio 1.75, the formation energy is positive at Cu rich limit and slightly negative at Cu poor limit. This implies acanthite like $Cu_{1.97}S$ is more probable than $Cu_{1.75}S$ and it does not prefer too many Cu vacancies.

Table 4-1 Defect formation energy for acanthite like at Cu-rich and Cu-poor limit using DFT.

Cu:S ratio	**Defect Formation Energy per Cu vacancy (eV)**	
	Cu-rich	**Cu-poor**
1.97	-0.367	-0.585
1.94	-0.0325	-0.186
1.91	-0.014	-0.184
1.75	0.111	-0.107

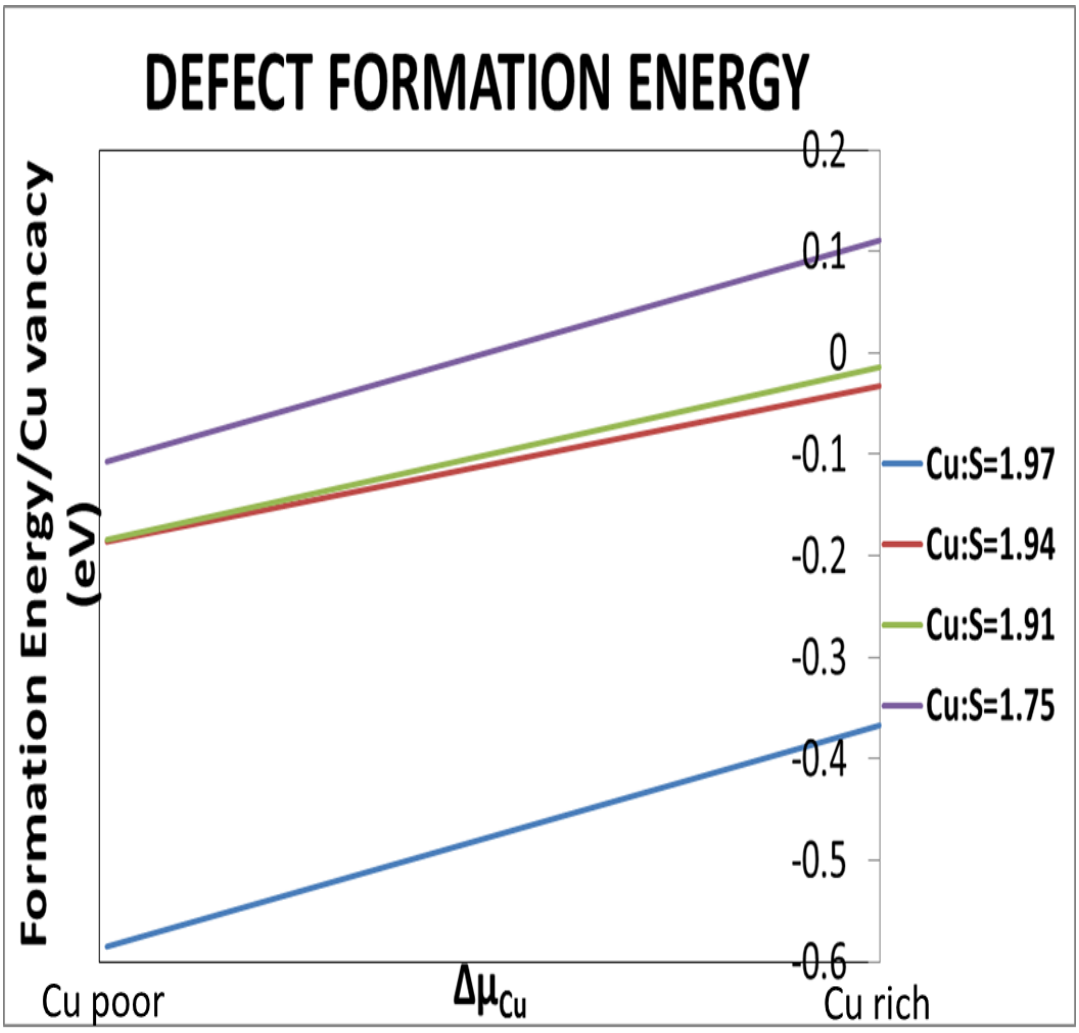

Figure 4-1 Defect formation energy per Cu-vacancy as a function of copper chemical potential for acanthite like structures for different V_{Cu} using DFT. Green line and red line almost fall together.

4.2.2 Cu bonding in Cu vacancy structure

There is high interaction between Cu-Cu atoms in Cu_2S structures as the bond distance between copper atoms are less than that observed in other copper compounds.

It may be highly possible that small Cu-Cu distance is playing a role in forming Cu-Cu vacancy as well. Hence, it is necessary to have a proper understanding of bonding in copper vacant structure. There is just slight change in volume with copper vacancies. The volume changes by 0.4 percentages in $Cu_{1.97}S$. Average Cu-Cu bond length seems to increase slightly as well with increasing copper vacancy. Average distance increases by .03 Å for $Cu_{1.97}S$ as compared with Cu_2S. This increment denotes that there is too high copper-copper interaction in Cu_2S which may facilitate copper vacancy in Cu_2S. Figure 4-2 shows the structure for $Cu_{1.97}S$ with Cu-Cu bonds using two different models. The structure still preserves the Cu-Cu layer which can be seen in Figure 4-2. The layer does break up with higher vacancies which will be shown shortly.

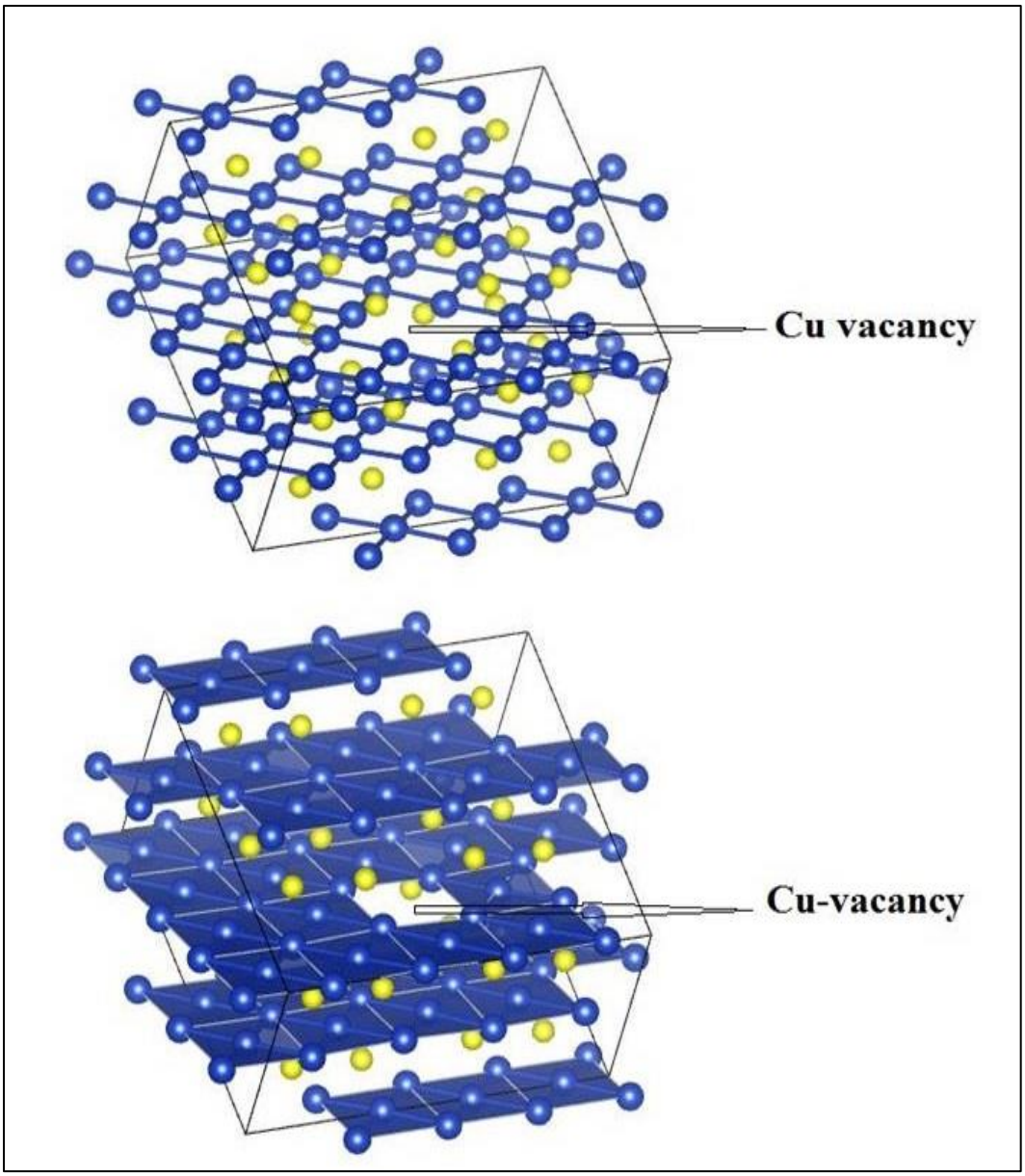

Figure 4-2 The two different models of DFT optimized structure for acanthite like based $Cu_{1.97}S$ are shown. The upper one is ball and stick model and the lower one is polyhedral method.

4.2.3 Acanthite like based $Cu_{1.75}S$

a) Stability

There are various Cu_xS structures that exist with different composition of x. According to the previous published literatures, anilite ($Cu_{1.75}S$) is the most stable structure in copper sulfide family [23, 24]. Hence it is important to study the structure with Cu to S ratio 1.75. We performed a DFT calculation on anilite and on $Cu_{1.75}S$ obtained from acanthite like. The heat of formation of anilite is -0.46 eV which is consistent with previously published DFT result on anilite [7]. Heat of formation is high for acanthite like ($Cu_{1.75}S$) which is -0.405 eV. The heat of formation of acanthite like ($Cu_{1.75}S$) is even higher than pristine acanthite like itself by 30 meV. This clearly indicates that anilite is more stable and acanthite like based $Cu_{1.75}S$ is unlikely to form which concord with the previously mentioned statement that acanthite like does not prefer high copper vacancy. The structures of anilite and acanthite like based $Cu_{1.75}S$ are shown in figure 4-3. Unlike in pristine acanthite like structure, Cu atoms are not arranged in layers in both $Cu_{1.75}S$ structures. The symmetry between copper atoms is broken in acanthite like structure with high copper vacancy.

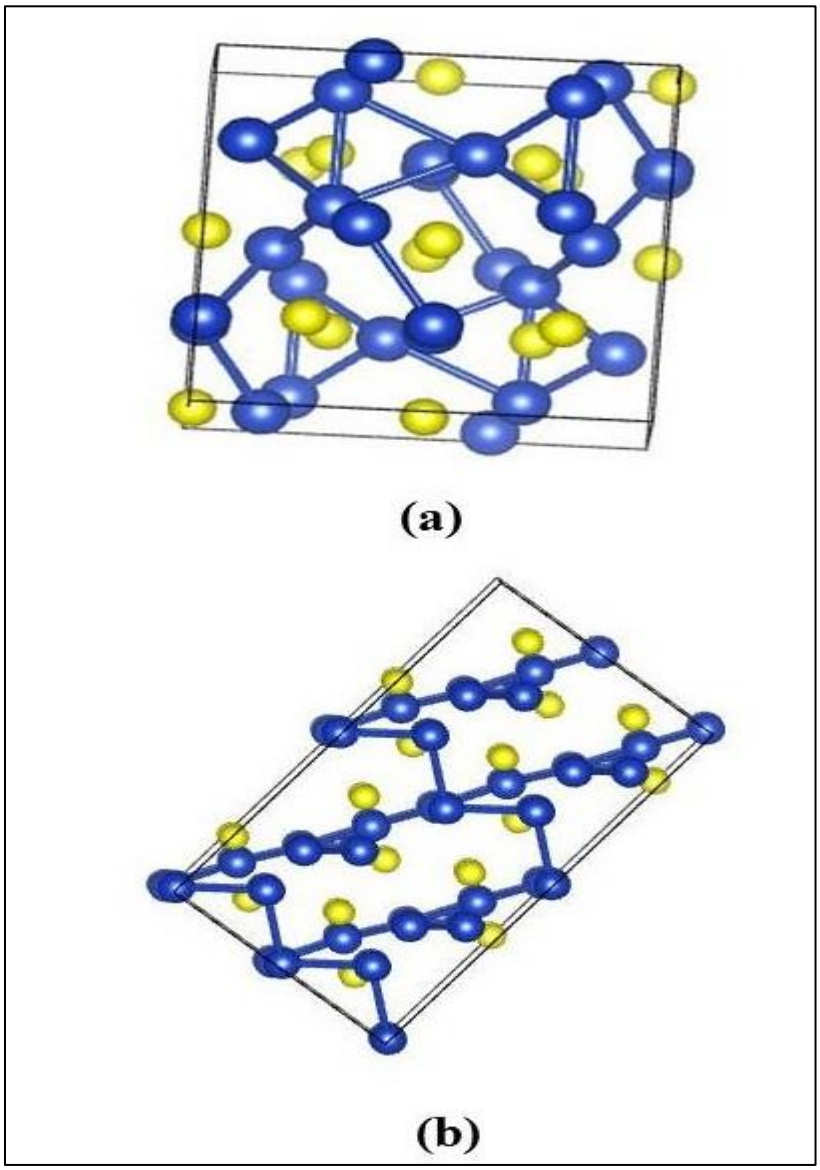

Figure 4-3 DFT optimized structure for $Cu_{1.75}S$. (a) is anilite and (b) is acanthite like based $Cu_{1.75}S$.

b) Electronic properties

Next we present electronic properties of acanthite like based $Cu_{1.75}S$. Here we are mainly comparing the electronic properties of pristine acanthite like Cu_2S and acanthite like ($Cu_{1.75}S$) to demonstrate the maximum contrast between stoichiometric and Cu vacant structure. Figure 4-4 shows the band structure for $Cu_{1.75}S$ calculated using DFT+U. Electronic calculation shows that band gap is 1.689 eV for $Cu_{1.75}S$ with U = 7 eV on Cu-d. The band gap opens up significantly with copper vacancy. The band gap is also direct in nature whereas band gap is indirect for acanthite like. It can be seen in figure 4-5 that Fermi level is moving in downward direction indicating the defect structure has become more p-type, as expected, due to the presence of hole in valence level. The lowering of Fermi level is helping to open up the band gap and the band gap opening is also seen in total dosplot (figure 4-6) and pdosplots (figure 4-7 and 4-8). The lowering of fermi level or valence band can be attributed to the weaker p-d hybridization in $Cu_{1.75}S$ than in Cu_2S which is clearly visible in copper pdos. We can see in total dos that a peak at around -2eV gets lowered in case of $Cu_{1.75}S$ indicating lower hybridization. There is slight changes at around fermi level with vacancy such as the contribution of Cu-p at conduction band decreases as structure becomes highly doped with holes but overall the features remain the same as still valence band is highly Cu-d dominant and S-p is playing a crucial role at conduction band.

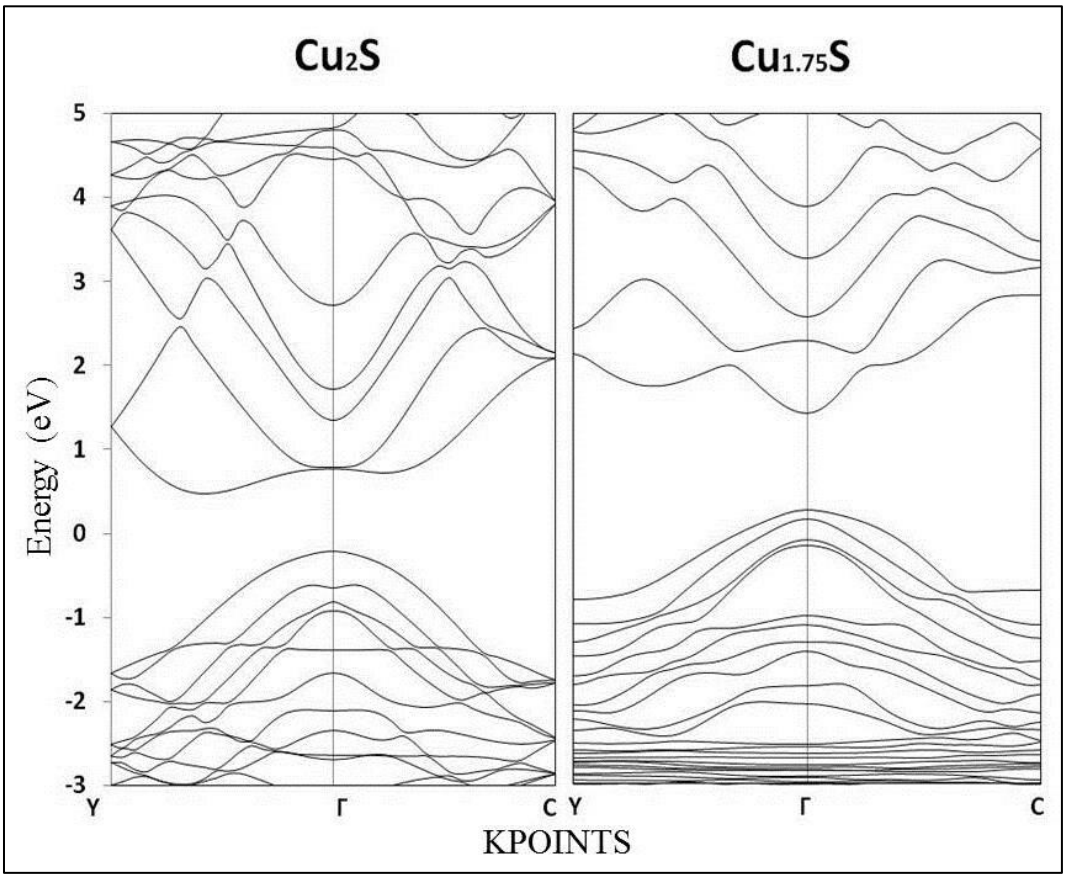

Figure 4-4 Band structure for Cu_2S(acanthite like) and $Cu_{1.75}S$(acanthite like based) using DFT + U = 7. The nature of band gap changes from indirect to direct with Cu vacancy.

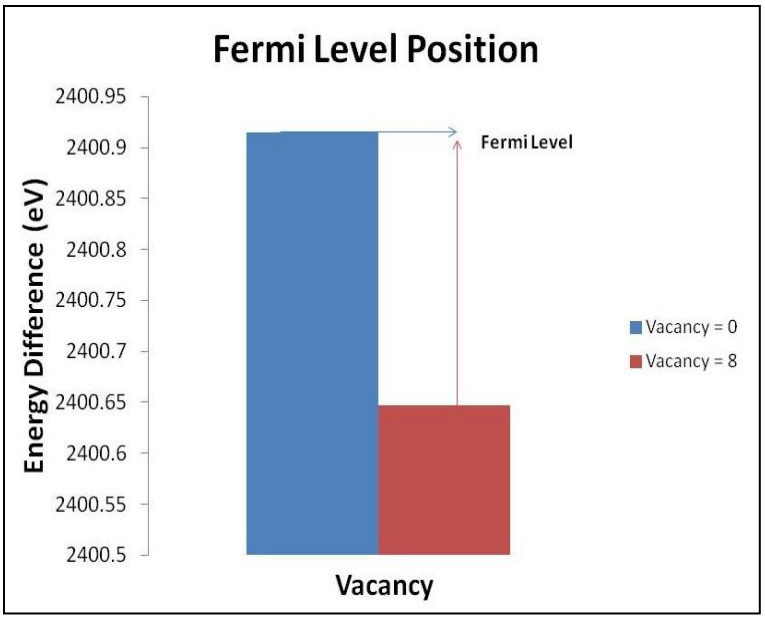

Figure 4-5 Fermi level as compared with innermost S-1s energy level. Vacancy = 8 denotes $Cu_{1.75}S$.

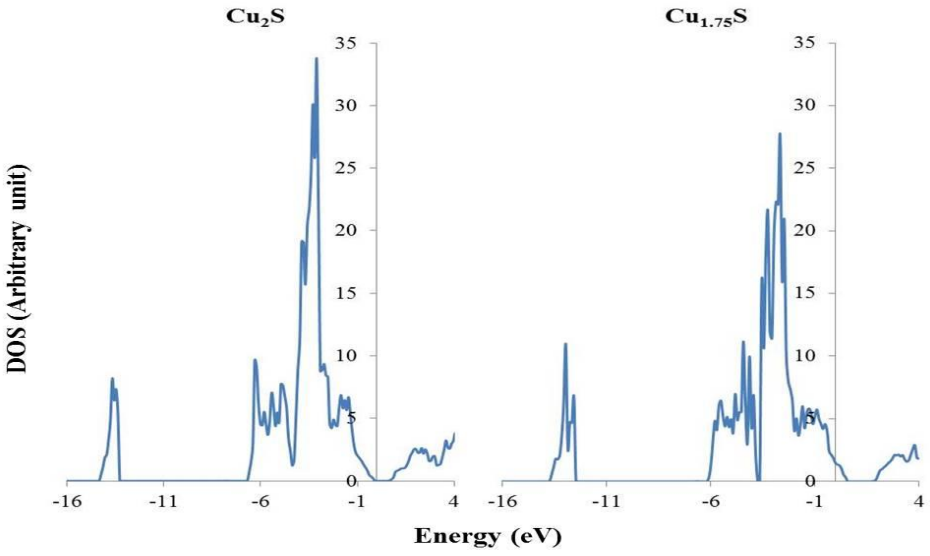

Figure 4-6 A comparison of DFT+U = 7 total dos between Cu_2S and $Cu_{1.75}S$.

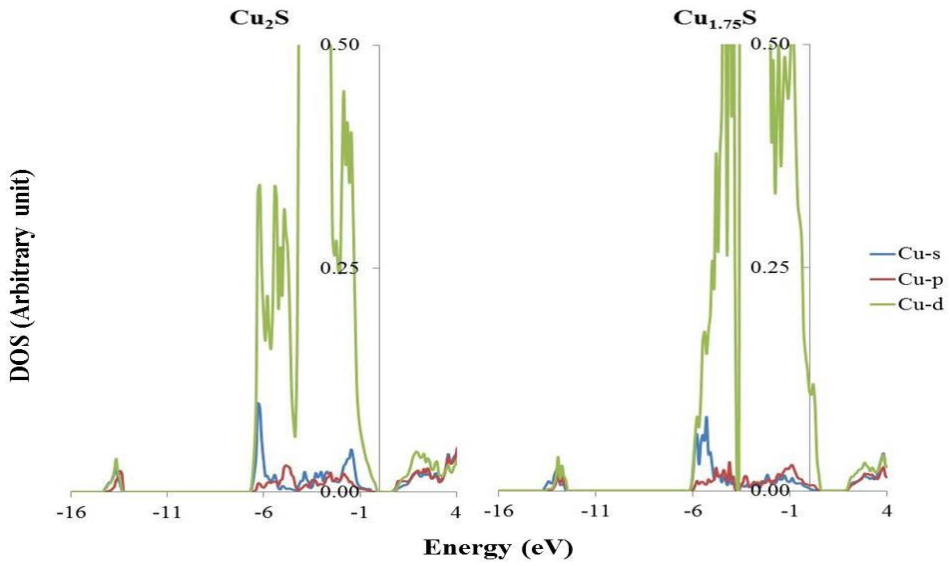

Figure 4-7 A comparison of DFT+U = 7 copper pdos between Cu_2S and $Cu_{1.75}S$.

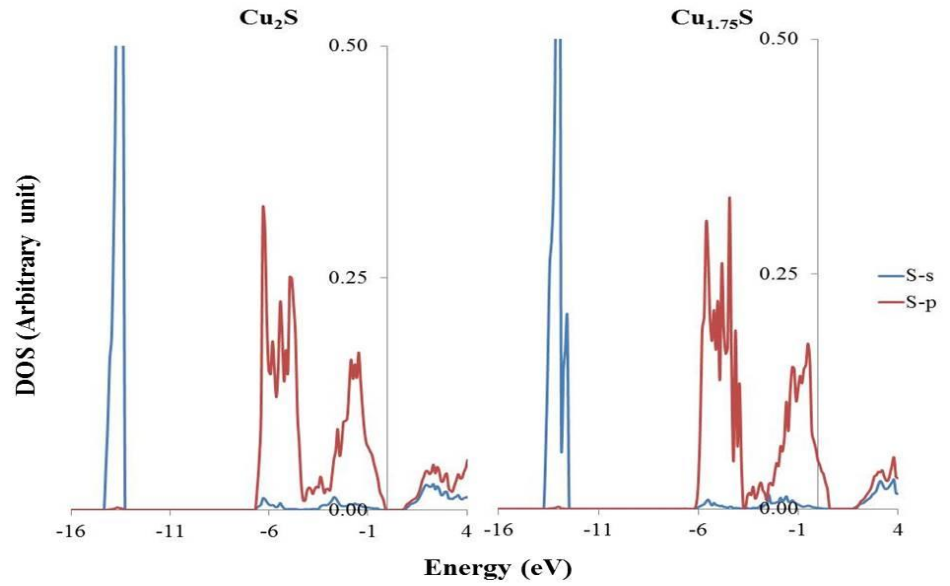

Figure 4-8 A comparison of DFT+U = 7 sulfur pdos between Cu_2S and $Cu_{1.75}S$.

4.3 Vacancy Formation in Low Chalcocite

4.3.1 Stability and comparison with acanthite like

So far we presented results for vacancy in theoretically favor copper sulfide structure. As we know low chalcocite is thermodynamically determined structure in experiment, we did study low chalcocite based Cu_xS structure as well by creating vacancy on it. We created different number vacancy in low chalcocite. Figure 4-9 compares heat of formation for different low chalcocite vacancy structure with acanthite like. Both low chalcocite and acanthite like show almost similar kind of behavior when vacancy increases. A decrease in heat of formation as x values decreases in Cu_xS indicates the tendency of both low chalcocite and acanthite like structure towards the formation of copper vacancy. With x values ranging from 1.97 upto atleast 1.91, heat of formation increases slightly. Similar kind of result is also observed from defect formation energy calculation on acanthite like based Cu_xS as shown in figure 4-1.

To get a clear picture let us just focus on $Cu_{1.98}S$. In order to find the probability of forming the defect structure at composition x = 1.98 from parent structure, we calculated the defect formation energy at two extreme cases. Figure 4-10 shows schematically the defect formation energy as a function of copper chemical potential for acanthite like ($Cu_{1.98}S$) and low chalcocite ($Cu_{1.98}S$). Defect formation energy figure reveals three important results: (i) The formation energy is lower at Cu-poor condition, (ii) the formation energy for low chalcocite ($Cu_{1.98}S$) is positive at Cu-rich condition whereas for acanthite like ($Cu_{1.98}S$) formation energies are negative at both cases, and (iii) At both Cu-rich and Cu-poor conditions, the defect formation energy of acanthite like ($Cu_{1.98}S$) is lower than that of low chalcocite ($Cu_{1.98}S$). The above mentioned points indicate that formation of acanthite like ($Cu_{1.98}S$) is thermodynamically more probable than low

chalcocite ($Cu_{1.98}S$). Such results depicts that although acanthite like structure is ground state structure of Cu_2S, it is also more prone to formation of copper vacancy and probably one of the reasons behind not observing acanthite like in experiment.

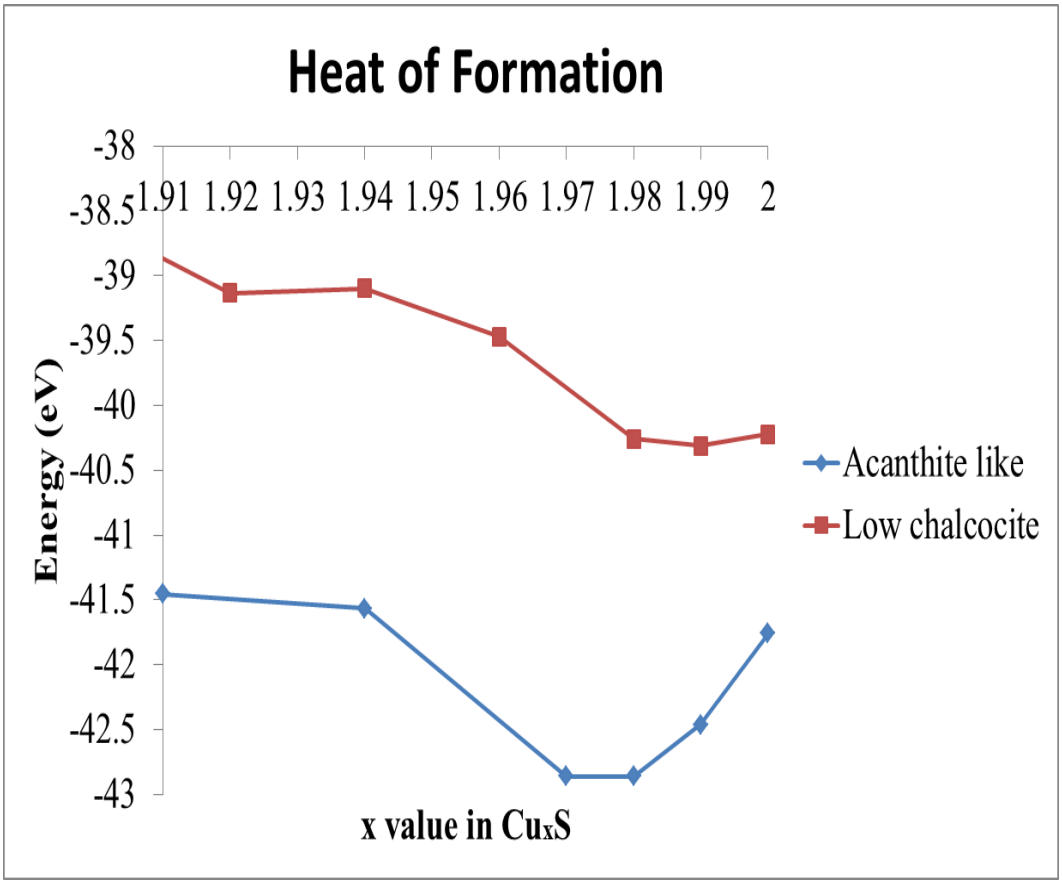

Figure 4-9 A line diagram for heat of formation trend for acanthite like and low chalcocite structures. Blue line is for acanthite like and red one is for low chalcocite. Energy is compared with respect to $Cu_{192}S_{96}$ atoms supercell.

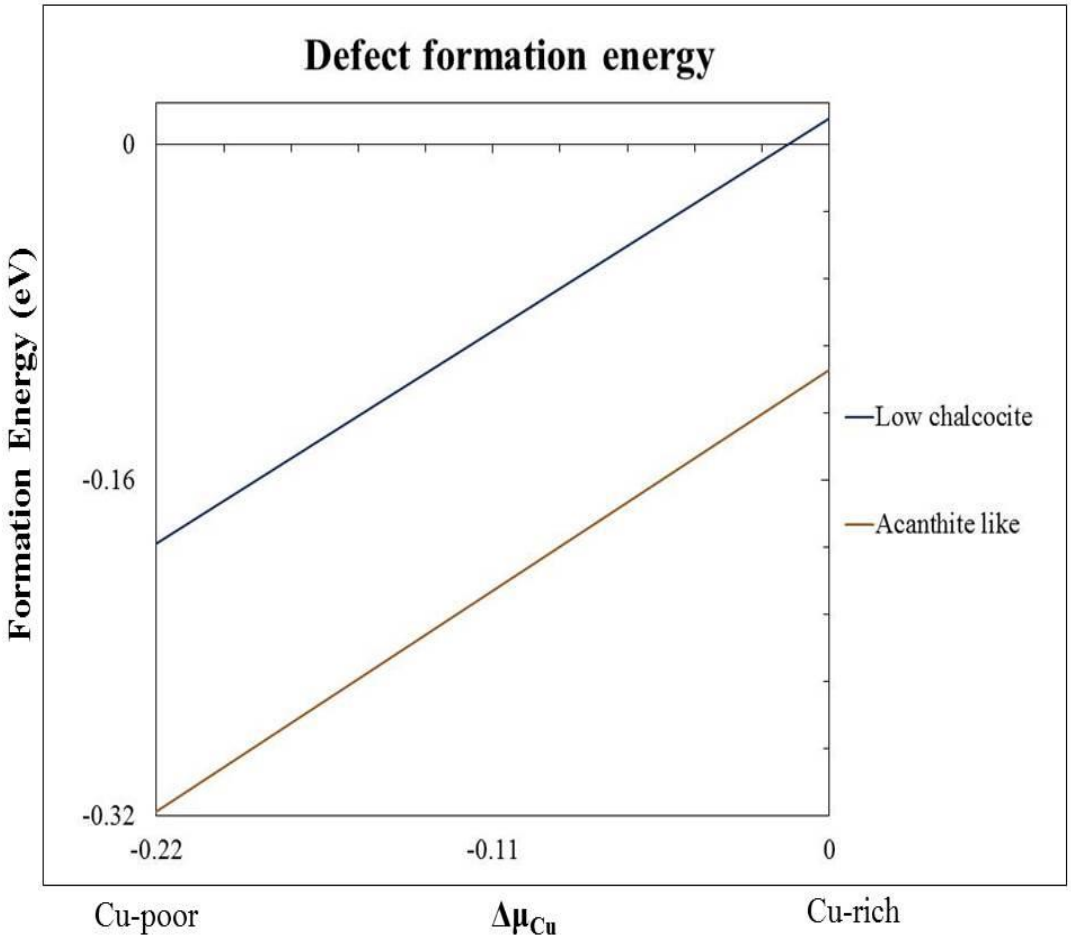

Figure 4-10 Defect formation energy for $Cu_{1.98}S$ as a function of copper chemical potential calculated using DFT

4.3.2 Molecular dynamics

Experimental work so far have only shown the occurrence of low chalcocite structure. We already provided one of the possible reason for it. Another possible reason behind such discrepancy between theoretical and experimental work can be the mobile nature of Cu atoms in Cu_xS. Due to this mobility of copper, copper atoms randomly

diffuses between different sites as reported by Ling-Wang Wang [68]. Moreover, he also claimed in his paper that at high temperature Cu_2S is a solid liquid hybrid phase. Acanthite like structure is stable at 0 K as DFT calculations are done at 0 K. A slight increase in temperature may cause copper atoms in acanthite like structure to move to different sites decreasing its stability and it is difficult to determine such structure experimentally.

To validate such prediction, we performed a molecular dynamics calculation on 144 atom structure with acanthite like atomic arrangement but with cell parameters of low chalcocite at around room temperature. The calculation is carried out in VASP using the projector augmented wave (PAW) method using generalized gradient approximation (GGA) method using density functional theory. Molecular dynamics is carried out using 3fs as the time step at 300K temperature. An energy cut of 400 eV is used for plane wave basis set.

We are mainly interested in the movement and position of copper atoms. In figure 4-11, it is clearly visible that copper atoms are arranged in layers initially. After performing molecular dynamics simulation at about room temperature, copper atoms diffuse from their positions showing self-diffusion. Cu atoms are not well organized and the Cu-Cu layer is broken. Moreover, the atomic arrangement inside the cell resemble low chalcocite to some extent after performing molecular dynamics at 300K as shown in figure 4-11. Hence, acanthite like structure is actually a ground state structure of Cu_2S at 0 K but due to mobility of copper inside the cell with the increase in temperature copper atoms diffuses to different sites because of which acanthite like structure has not been observed in experiment yet.

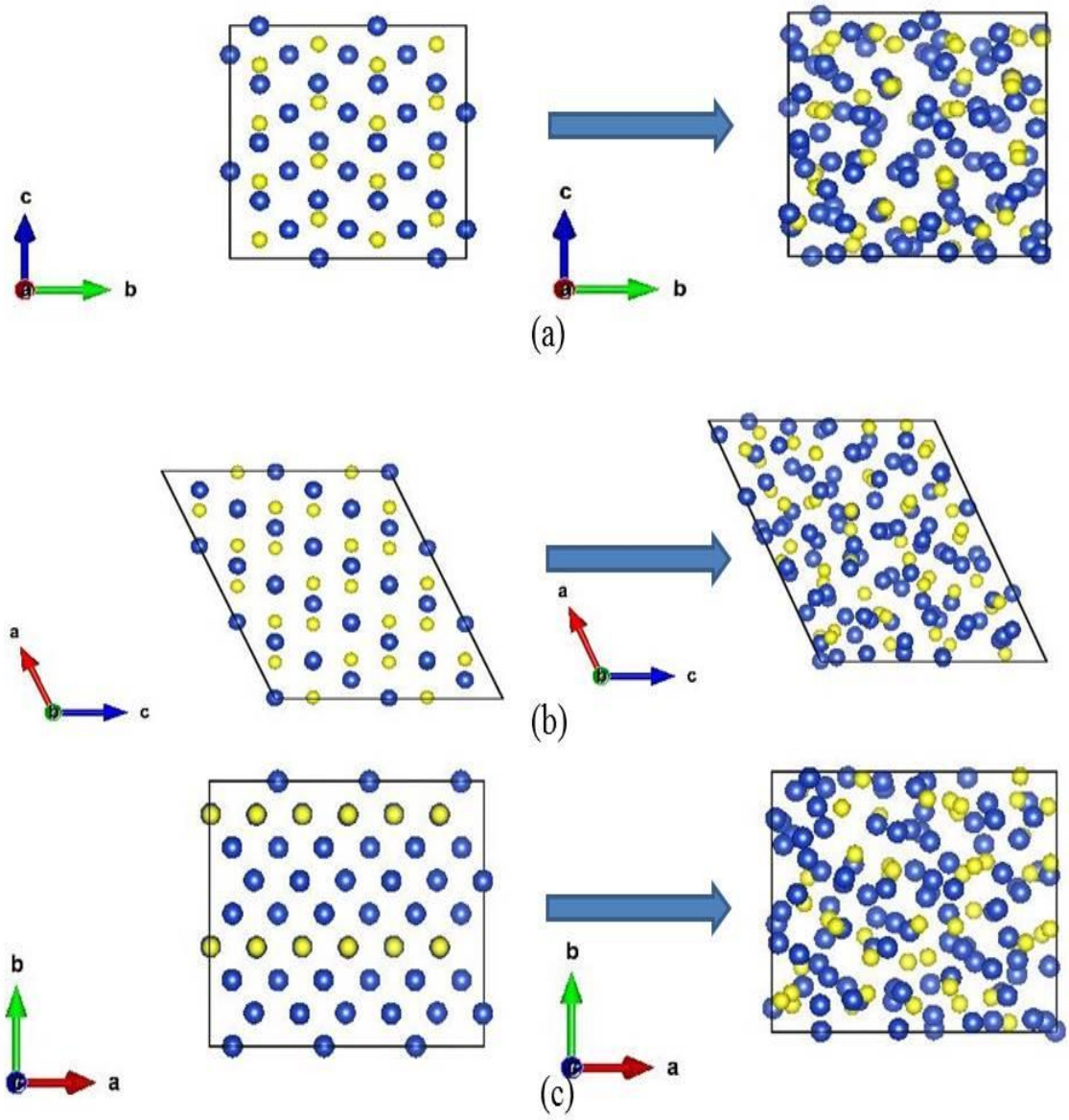

Figure 4-11 Diffusion of copper atoms inside the cell at room temperature. The structure on the left is initial structure and the right side structure is after performing molecular dynamics. (a), (b), and (c) denote different viewing directions.

4.3.3 Electronic properties of low chalcocite based $Cu_{1.98}S$.

a) Comparison with low chalcocite

Now we present electronic properties of low chalcocite based Cu_2S and $Cu_{1.98}S$ structure. The band gap obtained for low chalcocite is direct in nature and is consistent with previous results [23, 24, 68]. The calculated DFT band gap is 0.39 eV for low chalcocite which is significantly lower than experimental results. This may be due to limitation of DFT in predicting band gap. Low chalcocite based $Cu_{1.98}S$ has direct band gap as well which is also about 0.39 eV as shown in figure 4-12. The corresponding DOS is given in figure 4-13. Cu_2S and $Cu_{1.98}S$ have same band because the vacancy is so small that it does not affect the electronic properties considerably. We have already shown that large number of vacancy changes the band gap significantly.

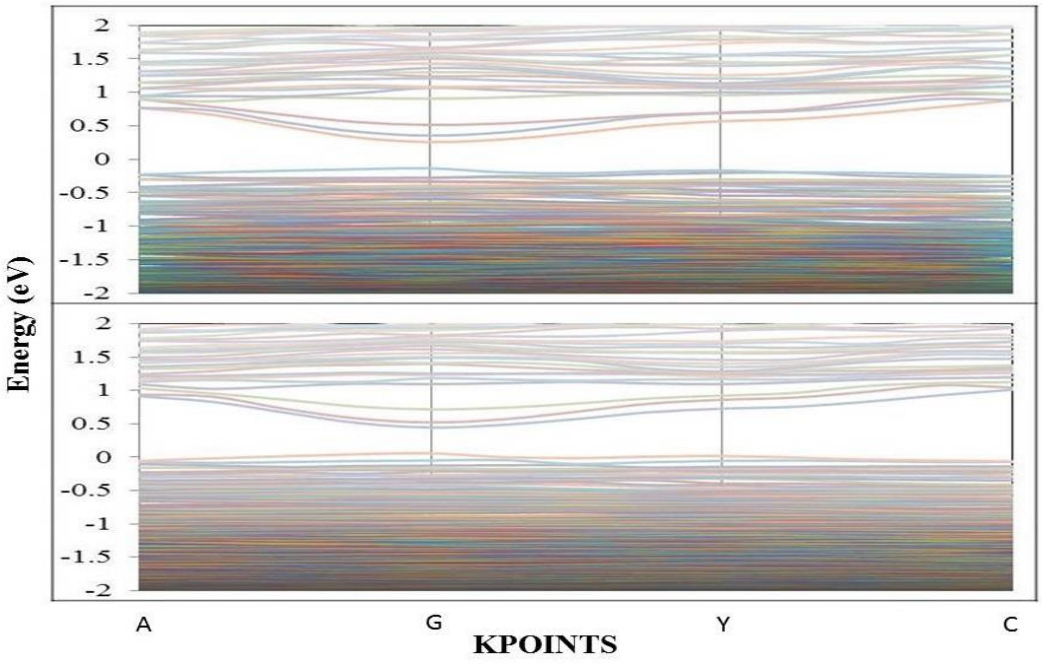

Figure 4-12 Band structure for low chalcocite based structure using DFT. The top structure is for Cu_2S and bottom one is for $Cu_{1.98}S$.

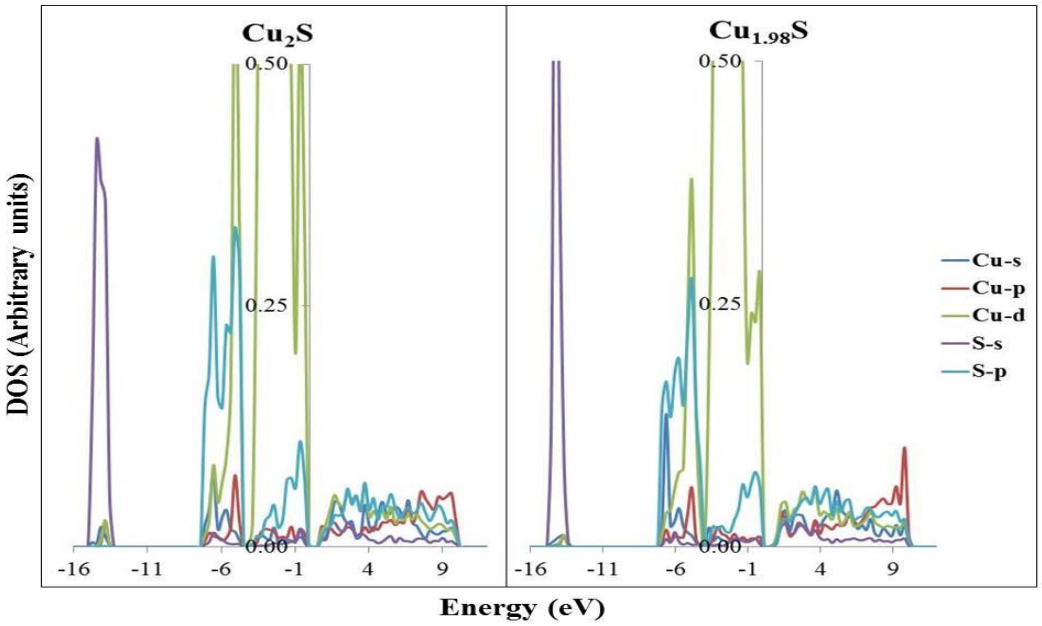

Figure 4-13 DFT partial dosplots for low chalcocite based Cu_2S and $Cu_{1.98}S$.

There has been an uplift of CBM in $Cu_{1.98}S$ structure. Similar kind of behavior was also observed in acanthite like based copper vacancy structure. The partial DFT dosplot is given in figure 4-13. Unlike in pristine Cu_2S structure, the bottom of conduction band is not only composed of Cu-p in $Cu_{1.98}S$ but also have contribution from Cu-s, Cu-d and S-p states. The top parts of the valence bands are formed due to hybridization of Cu-d and S-p but it mainly shows Cu-d characteristics as there is only little contribution from S-p in both structures. Similar kind of results was also observed in acanthite like structure. At around -6 eV, the contribution of S-p decreases whereas there is more contribution from Cu-s in $Cu_{1.98}S$ as compared with Cu_2S. The peak around -14.6 eV is due to S-s in both pdos. Overall the nature of density of states does not change much for low chalcocite based $Cu_{1.98}S$ as the vacancy is minimal.

As DFT is underestimating the gap, we did DFT+U calculation to see the change in band gap in $Cu_{1.98}S$. The band structure calculated using DFT+U is given in figure 4-14. The top one is DFT band structure and the bottom one is DFT+U. It is clearly visible that band gap shows significant increment with DFT+U as expected. DFT+U calculated band gap is around 0.74 eV. As in the case of acanthite like, with U parameter the conduction band moves up and also become less dispersive at gamma point suggesting increase in effective electron mass. There is no such remarkable difference in bands between DFT and DFT+U band structures other than increment in band gap.

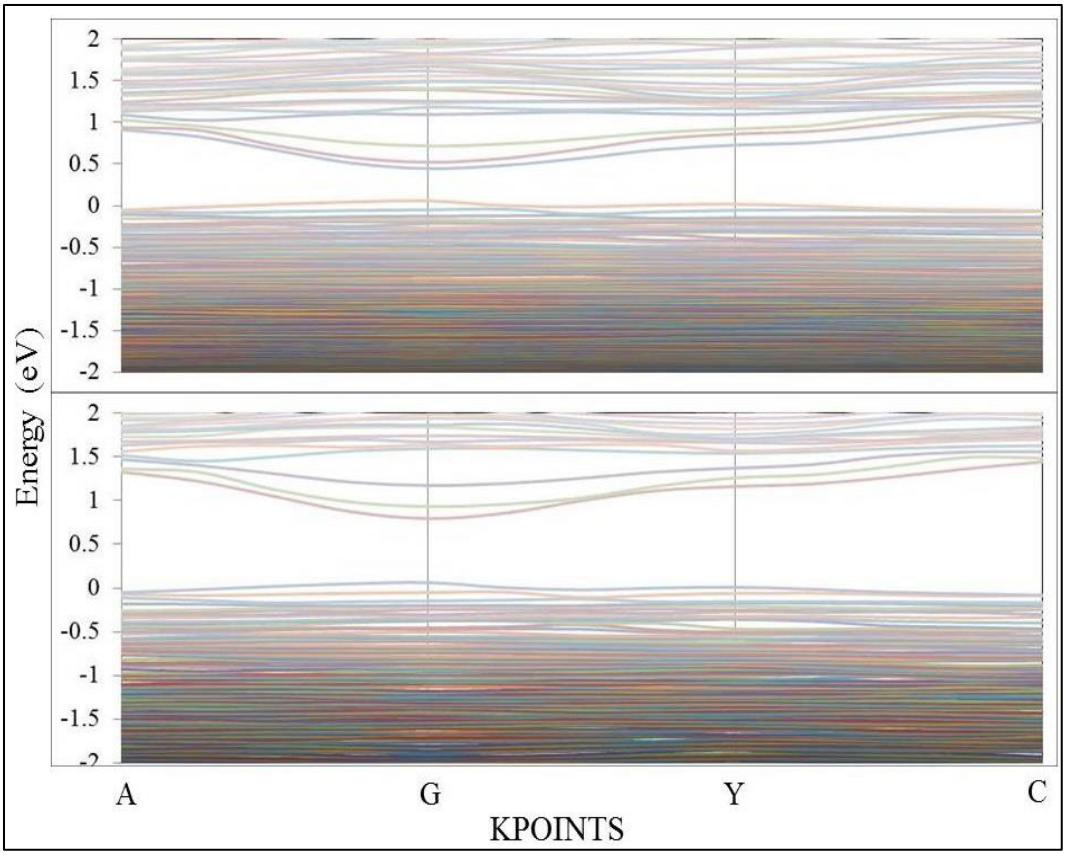

Figure 4-14 Band Structure for low chalcocite based $Cu_{1.98}S$. The top band structure is DFT calculated and the bottom one is DFT+U.

b) Comparison with acanthite like based $Cu_{1.98}S$

We already showed that acanthite like based $Cu_{1.98}S$ is more stable structure than low chalcocite based $Cu_{1.98}S$. Now we compare the electronic structure of the two. Since we know DFT is underestimating the electronic properties we only present DFT+U results here.

The band structure is given in figure 4-15. The band gap is direct and is about 0.74 eV in low chalcocite ($Cu_{1.98}S$) at gamma point whereas the gap is indirect and slightly larger (0.82 eV) in case of acanthite like ($Cu_{1.98}S$). CBM shows significance difference between two structures at gamma point. CBM is almost flat in acanthite like ($Cu_{1.98}S$) structure indicating high effective electron mass. Conversely, VBM is less dispersive in case of low chalcocite ($Cu_{1.98}S$) which means high effective hole mass in this structure.

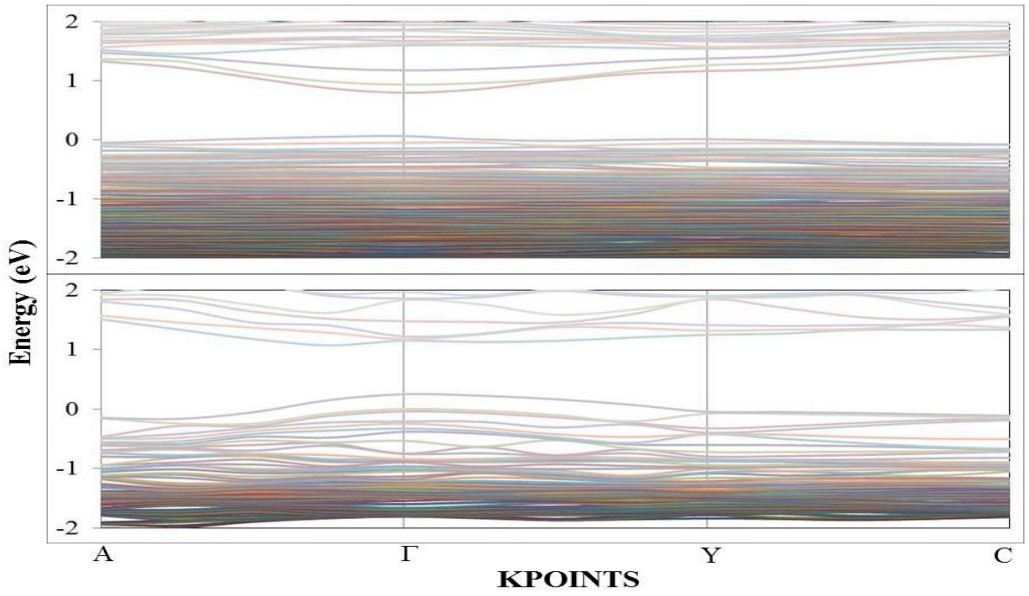

Figure 4-15 DFT+U band structure for $Cu_{1.98}S$ structures. The top one is for low chalcocite based and the bottom one is for acanthite like based.

The dosplots is given in figure 4-16. A small peak around 0 eV in acanthite like ($Cu_{1.98}S$) is due to the presence of hole state due to Cu vacancy. Interestingly such peak is not seen in low chalcocite based ($Cu_{1.98}S$). The valence band is formed by the hybridization of Cu-d and S-p with higher contribution from the former. The difference between two structures at valence level is the contribution form S-p orbital. Clearly, there is more S-p contribution in acanthite like ($Cu_{1.98}S$) in valence bands. There is a dominance of S-p in both pdosplots at conduction level. In low chalcocite ($Cu_{1.98}S$), CBM mainly shows Cu-p characteristics as in the case of pristine low chalcocite but acanthite like ($Cu_{1.98}S$) has more S-p dominance at CBM. Besides, in low chalcocite based structure the peak around -6 eV is due to S-p whereas in the case of acanthite like ($Cu_{1.98}S$) the peak is due to the hybridization of Cu-d and S-p.

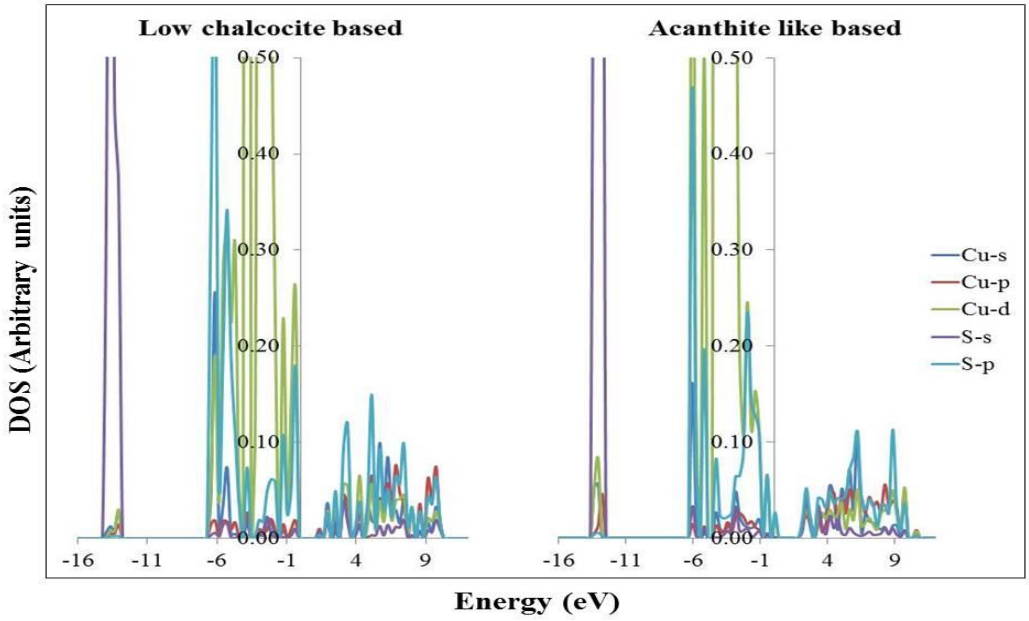

Figure 4-16 DFT+U partial dosplots for $Cu_{1.98}S$ structures. The left dosplot is for low chalcocite ($Cu_{1.98}S$) and right one is for acanthite like ($Cu_{1.98}S$).

4.4 Vacancy Formation in Str2

Str2 is another important structure to be discussed. The unit cell of str2 contains 4 Cu and 2 S atoms only and is one of the smallest unit cell structures among variety of structures considered with volume per formula unit of 49.31 $Å^3$. Energy of this structure is almost same as low chalcocite which makes this structure important. Although energetically they are similar, there is a huge difference between these two structures instead str2 is somewhat closer to acanthite like structurally as it also has copper layers present with average Cu-Cu bond distance of 2.61 Å.

We created a supercell for str2 and created vacancies on it. As in the case of acanthite like and low chalcocite, we took out different number of copper atoms from str2 supercell. Table 4-2 shows, with increasing vacancy, heat of formation increases for str2 based vacant structures. Such results suggest that str2 based vacant structures are not stable at all. This result is further strengthened by defect formation energy calculation. Figure 4-17 shows defect formation energy for str2. As expected defect formation energy is lower at Cu-poor condition but it is clearly visible in figure 4-17 that defect formation energy is positive at Cu-rich and Cu-poor limit and hence it is necessary to supply extra energy to create vacancy in str2. The result is quite unexpected for Cu_2S structure as acanthite like and low chalcocite both favors vacancy. More work is needed to be done on this structure in future to understand this seemingly uncertain behavior.

Table 4-2 Heat of formation for str2 based Cu_xS.

Cu:S ratio ≈	**Heat of Formation (eV)**
2	-0.420
1.96	-0.393
1.94	-0.387
1.88	-0.358

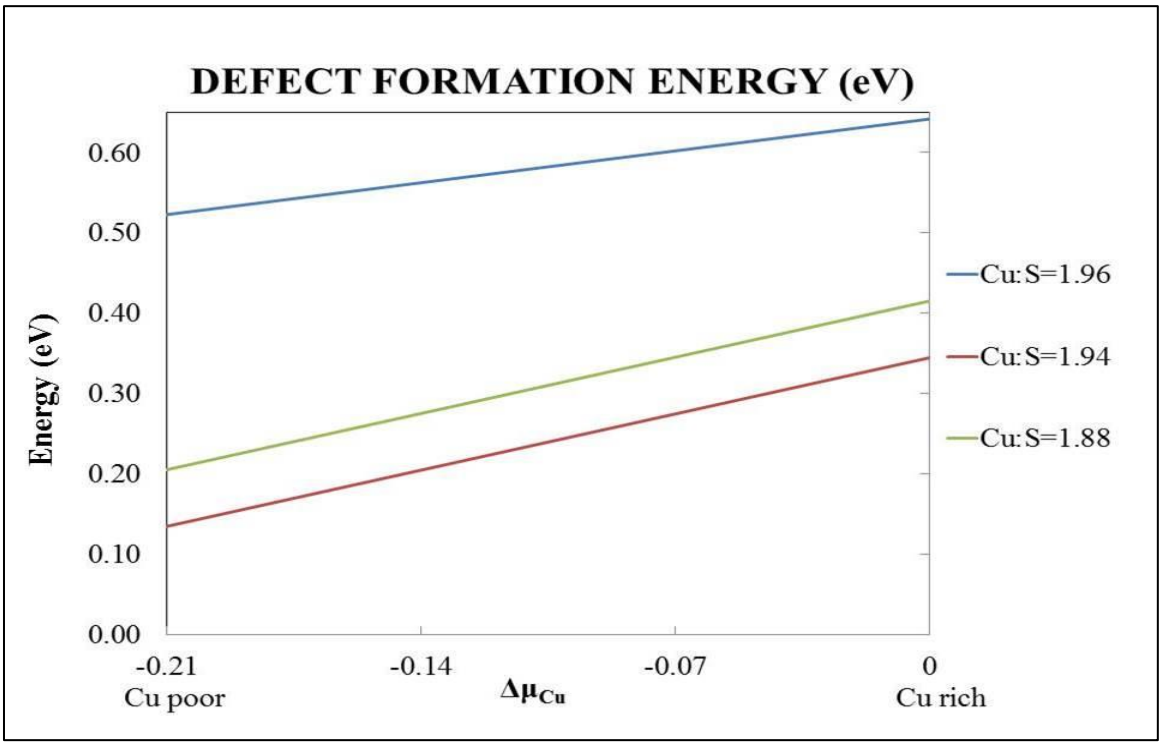

Figure 4-17 Defect formation energy for copper vacancy in str2 using DFT.

Chapter 5

Doping in Cu_2S

5.1 Introduction

In semiconductor industry, doping is another important factor. Doping intentionally introduces impurities into an intrinsic semiconductor for the purpose of modulating its properties mainly electrical properties. It is known that doping has improved the quality of many materials mainly in photovoltaic and electrical applications. Some of the popular doping materials are Indium (In), Aluminum (Al), Arsenic (Ar), Antimony (Sb), Tin (Sn), etc. Doping tin in oxides and sulfides is one of the common approaches to modify the properties of metal oxide/sulfide [69 - 73]. To the best of our knowledge no works have been reported on doping of Cu_2S with tin so as to modify its structural or electrical properties. In the present work we performed theoretical calculation on Cu_2S doped with Sn with the aim of focusing on two issues (i) stability and thermodynamic properties of Sn-doped Cu_2S, and (ii) the effect on Sn in the electronic properties. To study the electronic properties we also used DFT+U. Similarly, we also doped oxygen in Cu_2S to see how it affects Cu_2S thermodynamically and also to have theoretical consent in the experimental observance of copper vacancy formation in the presence of air.

5.2 Tin Doping

Tin (Sn) belongs to the group 14 in the periodic table. Sn has similar chemical properties like its neighboring element- germanium and lead. It has two possible oxidation states, +2 and the slightly more stable +4. Tin is obtained chiefly from the mineral cassiterite (SnO_2). Doping tin is one of the approaches in material science industry to improve the conductivity. Tin doping is highly favorable in many materials

such as TiO_2 because it has shown significant improvement in photocatalytic activities. As Cu_2S is not a stable material, doping can probably help to make it more stable and improve its properties. The success of tin doping on Cu_2S depends upon understanding the stability of a material and modification tin brings in electronic properties after doping.

5.2.1 Stability

There is no theoretical or experimental data on tin doping on Cu_2S yet. To examine how the concentration of Sn affects the stability and electronic properties, the Sn-doped structures were created for both acanthite like and low chalcocite. A 64 atoms supercell was created for acanthite like and 96 atoms cell was created for low chalcocite. Next we substitute 2, 4, 6, 8, and 10 Cu atoms with Sn to have abundant theoretical analysis to understand the stability of Sn-doped Cu_2S.

It is necessary to know how the doping structures behave energetically. First of all geometrical optimization was done by properly relaxing the structure by minimizing total energy and forces. To check the stability, we calculated the heat of formation and formation energies of the doped systems. The calculated heat of formation is summarized in table 5-1. Table 5-1 clearly reveals that the heat of formation decreases with increase of Sn content and the trend is similar for both theoretically and as well as experimentally favorable structure. The heat of formation per formula unit for 2 Sn-doped acanthite like and low chalcocite are -0.367 eV and -0.386 eV which is higher than that of their constituent Cu_2S. This shows that Sn-doped Cu_2S is not a stable material. This result is further enhanced after calculating the formation energies at Cu-rich and Cu-poor conditions. The formation energies for the doped system are calculated using the following formula

$$E_f = E_{tot}(D) - E_{tot}(0) + n\mu_{Cu} - n\mu_{Sn} \quad (5.1)$$

where $E_{tot}(D)$ is total energy of tin doped cell, $E_{tot}(0)$ is total energy of cell without doping, n is the number of Cu/Sn atoms removed/added, μ_{Sn} is the chemical potential of Sn and μ_{Cu} is the chemical potential of copper which depends upon its growth conditions.

Table 5-2 provides defect formation energies for Sn-doped Cu_2S which reveals following important information: (i) the formation energy is lower at Cu-poor condition for the substitution of Sn for Cu and (ii) the formation energy is positive at both Cu-rich and Cu-poor condition indicating the substitution of Sn for Cu is not energetically favorable. The radius of ionic Sn is less than that of ionic Cu, so substitution requires relatively more formation energy. The substitution of Sn for Cu is possible only if external energy is provided under suitable conditions but it is likely that it will show unusual characteristics as the material is not stable.

As we know copper sulfide (Cu_xS) prefers to stay at $x < 2$, we also did tin doping on acanthite like based Cu_xS structure to understand the stability of tin doping in copper deficit Cu_xS structure. Using supercell of acanthite like structure we created two different structures: first with one copper vacancy and second one with two copper vacancies. Then we did substitutional doping of tin replacing one copper atom in each structure. The heat of formation for the structure with one V_{Cu} is -0.410 eV and with two V_{Cu} is -0.414 eV. There is just a slight decrement in heat of formation with copper vacancy but still the heat of formation is higher than pristine acanthite like structure suggesting these tin doping structures are less stable than acanthite like itself. Hence, thermodynamically tin doping is not favorable in copper sulfide. Now it will be interesting to see if tin doping brings any positive results in improving electronic structure as it has done in materials like TiO_2 [71] and Ga_2O_3 [72].

Table 5-1 Heat of formation of Sn-doped Cu_2S

Number of Sn	**Heat of Formation per formula unit in eV (Acanthite like)**	**Heat of Formation per formula unit in eV (Low chalcocite)**
2	-0.367	-0.386
4	-0.365	-0.365
6	-0.380	-0.355
8	-0.340	-0.350
10	-0.326	-0.331

Table 5-2 DFT defect formation energies in Sn-doped Cu_2S under Cu-rich and Cu-poor conditions

Number of Sn	**Acanthite like- Defect formation energy per Sn substitution**		**Low chalcocite- Defect formation energy per Sn substitution**	
	Cu rich (eV)	**Cu poor (eV)**	**Cu rich (eV)**	**Cu poor (eV)**
2	1.136	0.918	0.830	0.62
4	0.606	0.389	0.689	0.479
6	0.337	0.1193	0.559	0.349
8	0.424	0.207	0.610	0.331
10	0.392	0.175	0.465	0.256

5.2.2 Electronic properties

As one of the important reasons of doping is to modify the electronic properties, we shall discuss about the electronic properties as well. First of all we study electronic properties of acanthite like by using DFT. DFT generated band structure is given in figure 5-1 with corresponding total dosplot in figure 5-2. As identification of the nature of bands is an important step, partial density of states (PDOS) is also provided in figure 5-3. Fermi level is set at zero point. There is high dominance of Sn-p at conduction band, similar kind of features has also been observed in another study of tin doping in Ga_2O_3 [72]. Due to the presence of Sn-s, there is a high peak at around -9 eV which was absent in intrinsic acanthite like. There is no band state between -14 ev to -9.2 eV. Similar kind of feature was also observed in intrinsic case. It is clearly visible in figure 5-1 that there is zero band gap which is further confirmed by dosplots in figure 5-2 and 5-3. The fermi level is intersected as shown in dos by Sn-p states. Moreover electronic structure study by DFT shows tin doping makes the material to behave like a metal. It may be due to limitation of DFT, i.e., underestimation of localization in d-orbital in DFT which usually shows a small band gap semiconductor as a metal. Hence, it seems necessary to study electronic properties of Sn-doped Cu_2S using DFT+U however we do not have any experimental data to compare our theoretical results.

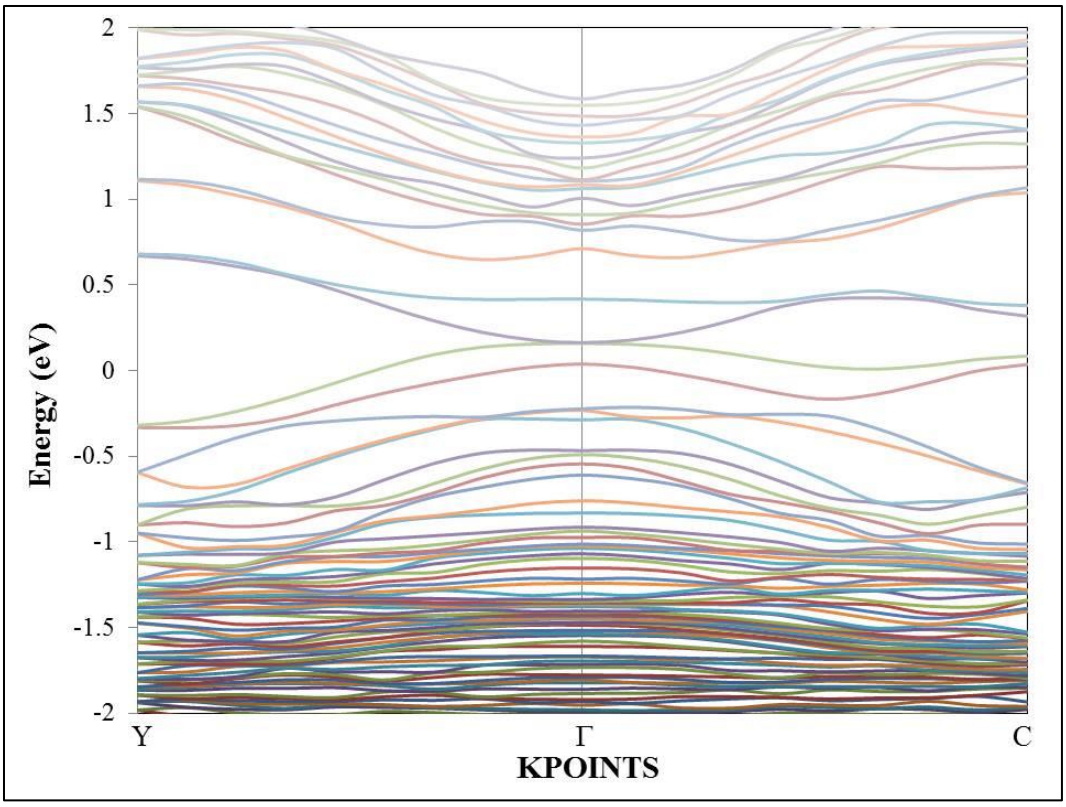

Figure 5-1 DFT band structure for 2 Sn-doped acanthite like.

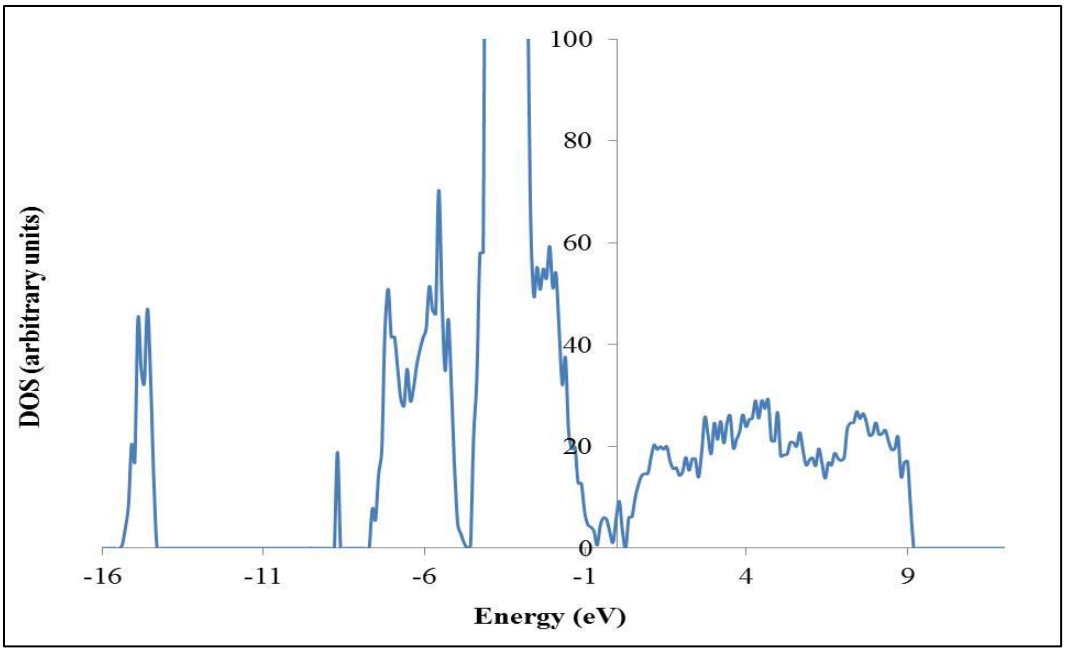

Figure 5-2 DFT total dosplot for 2Sn-doped acanthite like.

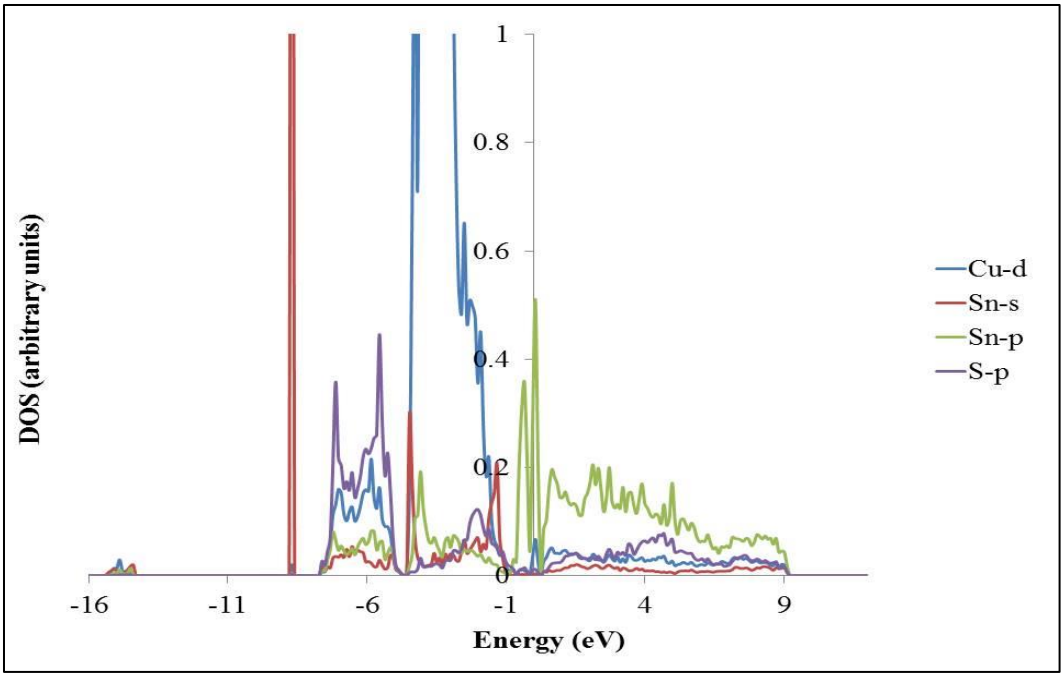

Figure 5-3 DFT partial dosplot for 2Sn-doped acanthite like.

Figure 5-4 shows the DFT+U band structure for 2 Sn-doped acanthite like structure followed by total and partial dosplots in figures 5-5 and 5-6 respectively. As compared with intrinsic acanthite like dosplots, there are only few changes in dosplots and the change is mainly around the valence and conduction level. There is no gap state in Sn-doped Cu_2S between -13.3 to -8.5 eV. Similar kind of no gap state was also observed in intrinsic Cu_2S. The overall shape of dosplots do not change much after doping hence we increase the resolution of dosplots to better see the activities near Fermi level. The only modified feature not seen in the dosplot due to increment in dos resolution is a peak around -8.4 eV due to Sn-s; similar to the peak shown in figure 5-3.

The Fermi level is set at zero point energy. With the introduction of the Sn, it can be clearly seen that the Fermi level is intersected with the impurity level as shown in band structure figure. The conduction band minimum (CBM) and the valence band maxima (VBM) has a band gap of 0.230 eV which is smaller than band gap 0.694 eV of intrinsic Cu_2S structures in which doping is done. Hence, there is no improvement in bang gap opening with tin doping rather the band gap decreases. There are impurity energy levels at the top of valence and the bottom of conduction bands which is mainly composed of Sn-s and Sn-p respectively. The flat nature of VBM and CBM indicates high effective masses for holes and electrons respectively. The energy of the valence electrons of Cu-d is reduced which is clearly shown in the dosplots as the DOS shifted towards the low energy direction by 1.30 eV. Hence, Cu-d is only dominant below -1.30 eV at valence band. The conduction band is predominantly Sn-p with very small contribution from Cu-d and Sn-s. The changes in the electronic structure near Fermi level is mainly due to the contribution from tin orbitals but the change is not suitable from photoconductivity point of view.

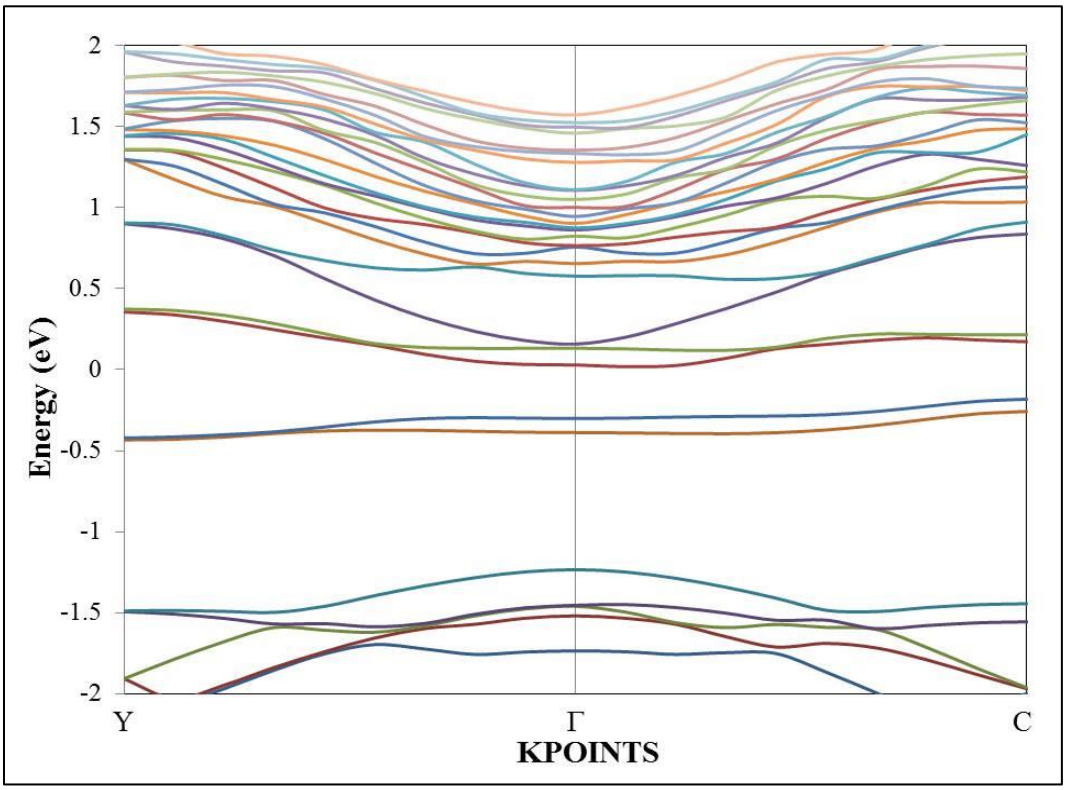

Figure 5-4 DFT+U band structure for 2 Sn-doped acanthite like structure.

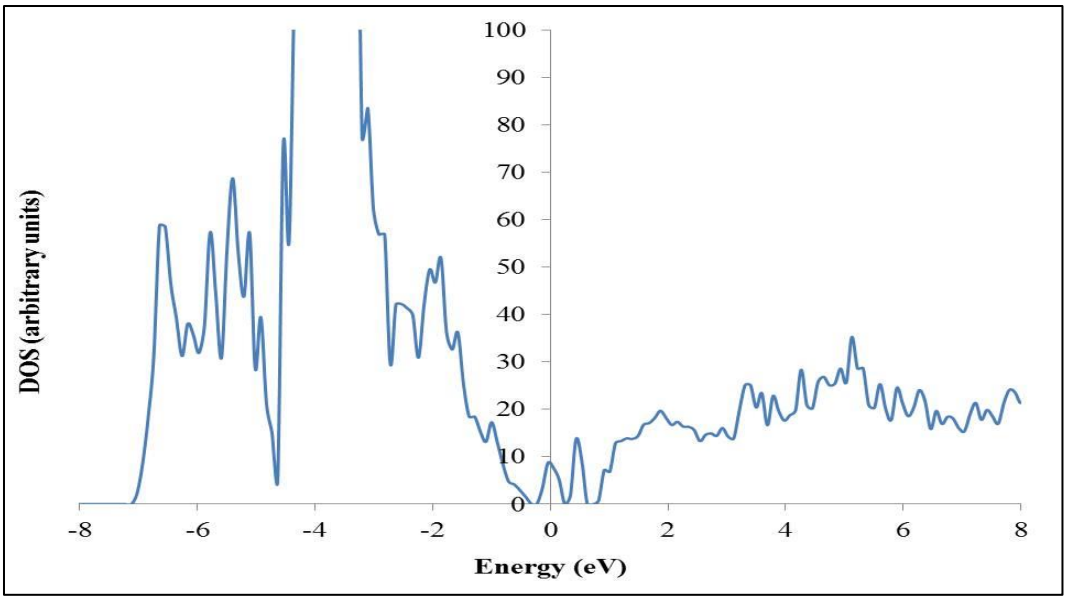

Figure 5-5 DFT+U total dosplot for 2 Sn doped acanthite like structure.

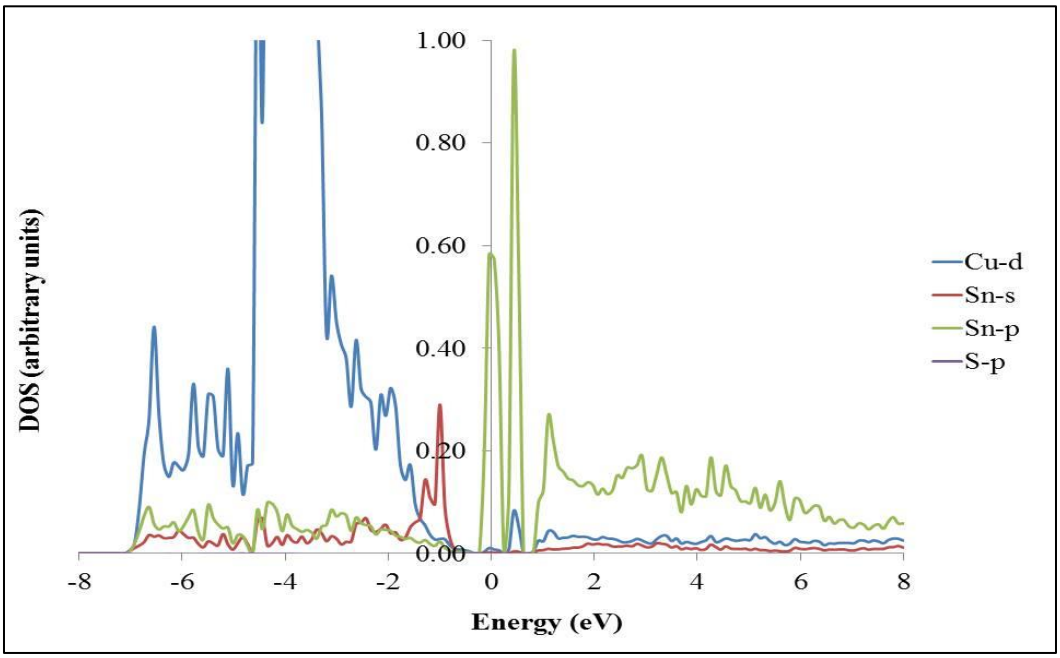

Figure 5-6 DFT+U partial dosplot for 2 Sn doped acanthite like structure.

Now we present DFT+U band structure and dosplots for 2 Sn-doped low chalcocite structure. The band structure is provided in figures 5-7 and corresponding dosplots are given in figures 5-8 and 5-9. There is no such significant difference between electronic structure of 2 Sn-doped acanthite like and 2 Sn-doped low chalcocite. The band gap is lower than the band gap of intrinsic low chalcocite similar to the case of acanthite like. Also VBM and CBM are less dispersive because of which effective hole and electron masses are high. Due to the presence of tin, as expected the Fermi level is intersected with impurity in low chalcocite as well. Sn-s is present at valence level whereas and Sn-p is dominant at conduction bands. Sn-s and Sn-p are playing the same role in tin doped low chalcocite as in acanthite like around Fermi level. In low chalcocite and acanthite like tin doping failed in bringing any effective change in electronic structure.

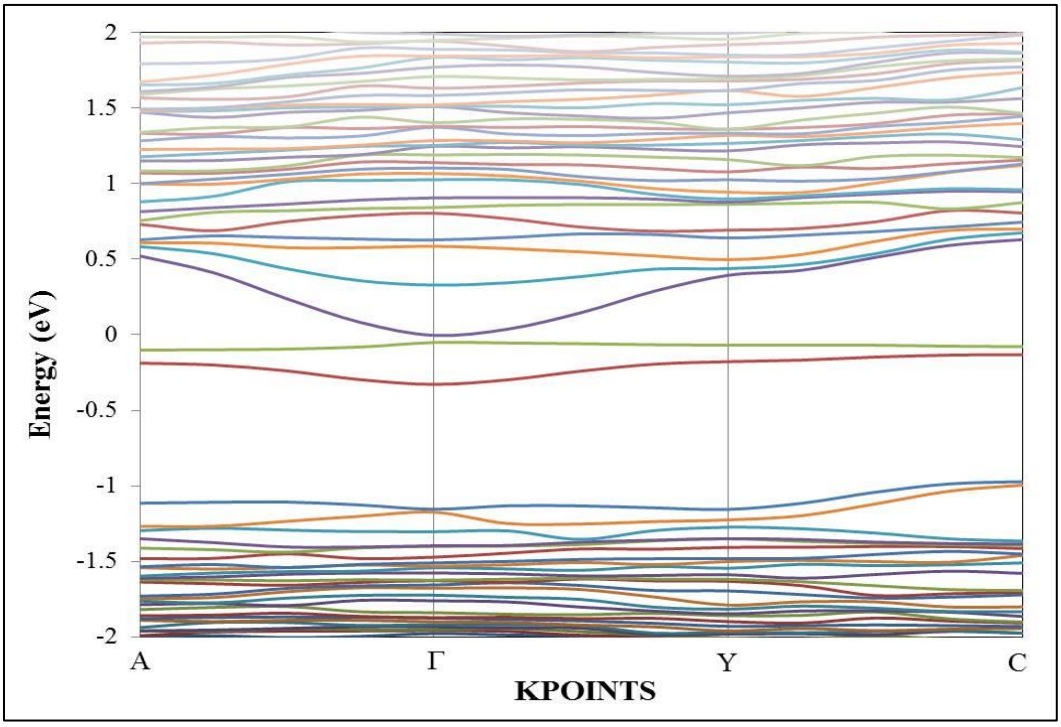

Figure 5-7 DFT+U band structure for 2 Sn doped low chalcocite structure.

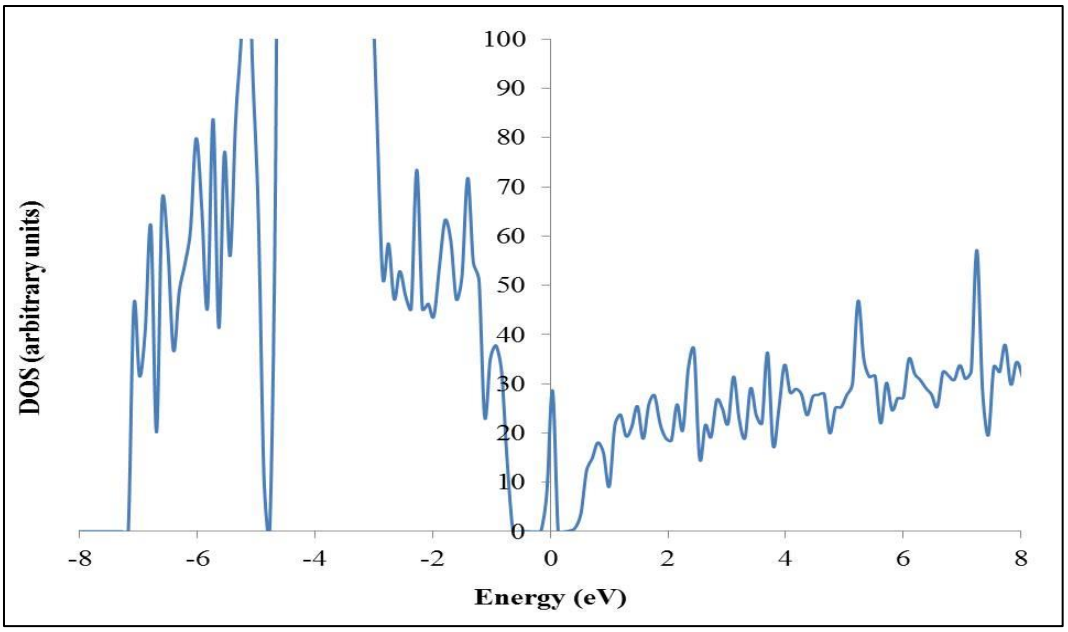

Figure 5-8 DFT+U total dosplot for 2 Sn doped low chalcocite structure.

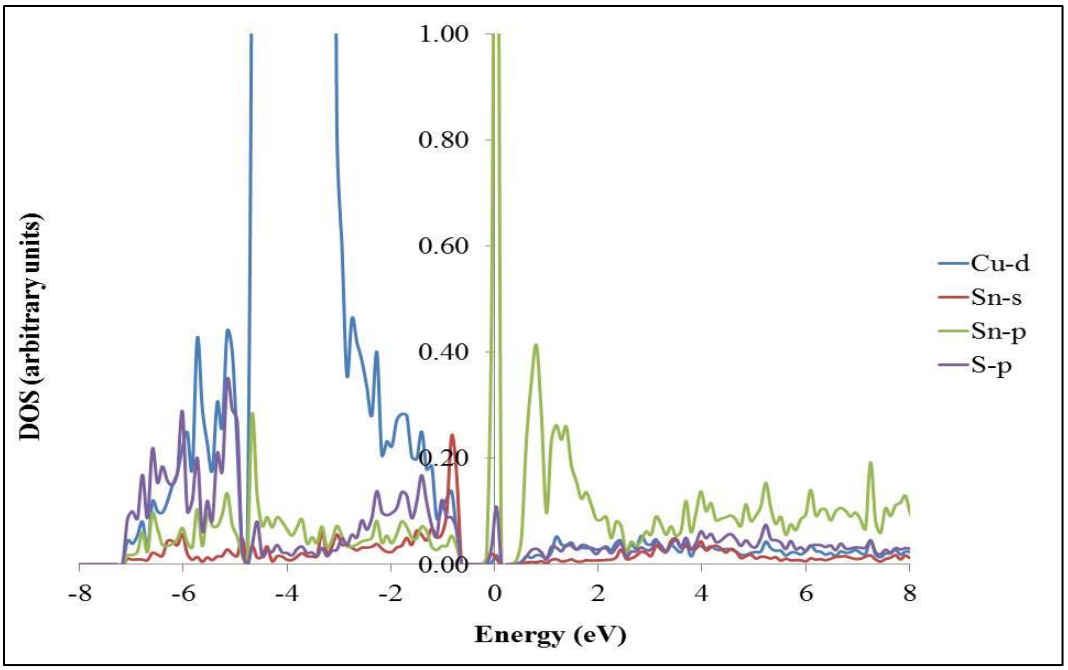

Figure 5-9 DFT+U partial dosplot for 2 Sn doped low chalcocite structure.

Similarly, band structure of tin doped in copper vacant (1 V_{Cu}) acanthite like structure shows similar features as without vacancy. The band structure for tin doped with one copper vacancy acanthite like based structure is shown in figure 5-10. There are band states present near fermi level due to the presence of tin as in all tin doping cases. Even tin doping in copper vacant structure could not improve the band gap and electronic properties. Hence, tin doping in copper sulfide is not suitable for photovoltaic application.

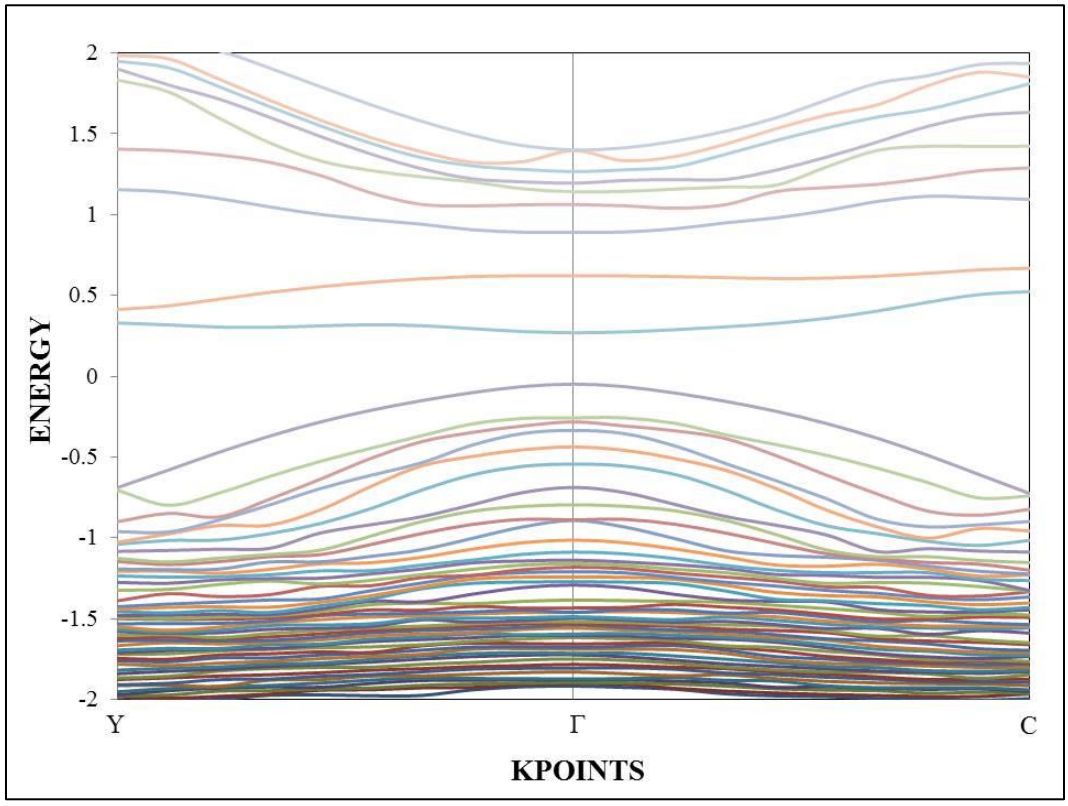

Figure 5-10 DFT+U band structure for Sn doped acanthite like structure with one copper vacancy.

5.3 Oxygen Doping

Oxygen is abundantly present in nature. Previously we discussed that Cu_2S is highly unstable in the presence of air and it forms vacancy instantly. Here, we used somewhat unconventional approach by doing substitution doping of oxygen for Sulfur in order to do theoretical verification of Cu vacancy formation in Cu_2S in air as claimed so far.

As our main purpose is to understand the behavior and stability of copper sulfide in oxygen rich environment, we just used acanthite like structure for this purpose. We already know that, from previous chapter, acanthite like favors copper vacancy. At Cu:S ratio 1.97, i.e. 1.6% Cu vacancy, the heat of formation is -0.447 eV. Figure 4-9 in previous chapter reveals that on further increasing the vacancy above 1.6% on acanthite like the heat of formation slightly increases too.

To understand the effect of O-doping in Cu_2S, we created two different acanthite like based O-doped structure: one without Cu vacancy and one with 6.25% Cu-vacancy. The structures were relaxed fully using DFT approach. Heat of formation and formation energies for the above mentioned structure is provide in table 5-3. The heat of formation for O-doped structure without Cu vacancy is -0.453 eV and with copper vacancy is -0.475. The O-doped structure with 6.25% Cu vacancy structure is not only more stable than the O-doped structure without any Cu vacancy but also more stable than any Cu vacant acanthite like structure without oxygen doping. This is consistent with the experimental results as in presence of oxygen, Cu vacant structure is more stable. The formation energies reveals the following features: (i) The formation energies for substitution of O for S is much lower than substitution of Sn for Cu, (ii) the defect formation energy decreases with Cu vacancy at both Cu-rich and Cu-poor conditions, and (iii) again at Cu-poor condition the defect formation energy has shown a considerable

decrement in copper vacancy structure. Such results indicate high probability of forming copper vacant structure in presence of oxygen. Hence, heat of formation and formation energy calculation both show agreement with experimental results that Cu vacant structure is more stable in presence of oxygen.

Table 5-3 Heat of formation and formation energy in O-doped acanthite like structure with and without Cu vacancy

Number of Cu Vacancy	**Acanthite like**		
	ΔH (eV)	Defect formation Energy (eV)	
		Cu-rich	Cu-poor
0	-0.453	-0.5670	-0.1230
4	-0.475	-1.226	-1.661

Chapter 6

Conclusion and Future Directions

6.1 Conclusion

The main focus of our research is to understand the stability issue of Cu_2S. As there is no proper theoretical background on ground state structure of Cu_2S, we used DFT to predict the most favorable stoichiometric Cu_2S structure, and then study its electronic properties and stability. We studied fifteen possible Cu_2S structure by gathering information from various resources. According to our DFT calculation, acanthite like structure has the minimum energy among all structures at 0 K which makes it the most probable stoichiometric ground state Cu_2S structure, even more favorable than low chalcocite. The result is further strengthened by DFT+U calculations. The presences of copper layers in acanthite like structure, which is absent in low chalcocite, and occupation of more volume per primitive cell in acanthite like structure seem to create a difference in energy minimization. Both structures are monoclinic in nature and interestingly average Cu-Cu bond distance is about 3-3.5% higher than that of metallic Cu-bond length showing high Cu-Cu interaction in Cu_2S as compared with other copper compounds.

Although acanthite like structure is the minimum energy structure predicted theoretically, it is still not observed in experiment. One reason behind this is acanthite like structure tendency towards the formation of copper vacancy as it would form vacancies spontaneously at any growth condition. Another important reason is copper atoms high mobility in Cu_2S and at slightly larger temperature Cu atoms move to take different possible Wyckoff sites. Calculations show that both acanthite like and low chalcocite structures show a tendency of forming copper vacancy but interestingly another structure,

str2, closest in energy to low chalcocite does not favor vacancy. More study is needed to be done in this structure as this is showing an opposite trend.

The study of electronic structure shows that most of the properties of Cu_2S/Cu_xS are determined by Cu-d orbital as it is dominant near Fermi level: VBs is dominated by Cu-d whereas CBs are formed by hybridization of different orbitals but show more S-p type features. DFT underestimates the band gap as expected and use of DFT+U and DFT-hybrid increases the band gap. The increase in band with U parameter is both due to downward shift of valence band and upward shift of conduction band. Most of the features of band structure are similar in all three calculations, DFT, DFT+U and DFT-Hybrid, with slight changes in the nature of conduction band with DFT+U and also in Hybrid calculations. With increasing vacancy in Cu_2S band gap increases and the increment is causing due to change in p-d hybridization. Overall, the study of electronic structure has shown that acanthite like and low chalcocite show many similar characteristics.

In order to see effect of doping in Cu_2S, Sn is used as a substitutional dopant in Cu_2S substituting Cu. Heat of formation of Sn-doped Cu_2S increases with increase of tin amount and defect formation energy is positive at both Cu-rich and Cu-poor limit. There are few changes in the electronic structure due to the presence of impurity level around Fermi level but overall electronic properties do not show improvement in its characteristics with tin doping. This highly suggests that tin cannot be a suitable doping candidate for Cu_2S. On the other hand use of oxygen as a dopant is highly favorable. The heat of formation and defect formation energy indicate that O-doped Cu_2S with copper vacancy is highly stable compound. This further strengthens the fact that Cu_2S is unstable towards the formation of Cu vacancy in presence of air.

In conclusion, we proposed a new ground state structure for Cu_2S theoretically. A systematic study has been done on understanding the electronic properties of Cu_2S. Although acanthite Cu_2S crystal structure is simpler than low chalcocite, their electronic structures are similar in nature. Molecular dynamics calculation shows that the structural difference in acanthite Cu_2S and low chalcocite is mainly due to mobility of Cu atoms inside the cell. Copper vacancy is inevitable in Cu_2S so it is necessary to find a proper doping material in order to stabilize Cu_2S and at the same time improve its efficiency in PV cells.

6.2 Future Directions

As temperature plays a crucial role in Cu_2S, more molecular dynamics calculations are needed to be done in future to know more about the structure and Cu movement in detail. Moreover, a proper study is needed to be done on high chalcocite and cubic phase using molecular dynamics. Similarly it is important to study str2 in details in future as this structure is showing opposite behavior than acanthite like and low chalcocite. Besides, it is necessary to resolve the issue of stability by finding a proper dopant so that Cu_2S can be more useful in PV applications.

References

1 E. Becquerel, Compt. rend. **9**, 561 (1839).

2 R. Williams, J. Chem. Phys. **32**, 1505 (1960).

3 A. Smith, Eng. Gas Turbines Power **91**, 1 (1969).

4 P. Joshua, Futures **34**, 663 (2002).

5 M. Bazilian, I. Onyeji, M. Liebriech, I. MacGill, J. Chase, J. Shah, D. Gielen, D. Arent, D. Landfear, S. Zhengrong, Renew. Energy **53**, 329 (2013).

6 Global Market Outlook for Photovoltaics 2014-2018, EPIA, visit www.epia.org.

7 Market Report 2013 (02), EPIA, visit www.epia.org.

8 J. Zhao, A. Wang, and Martin A. Green, F. Ferrazza, App. Phys. Lett. **73**, 1991 (1998).

9 J. Martin, Solar Choice (2012).

10 K. W. J. Barnham, G. Duggan, J. Appl. Phys. **67**, 3490 (1990).

11 A. Chirilă, P. Reinhard, F. Pianezzi, P. Bloesch, A. R. Uhl, C. Fella, L. Kranz, D. Keller, C. Gretener, H. Hagendorfer, D. Jaeger, R. Erni, S. Nishiwaki, S. Buecheler, A. N. Tiwari, Nature. Mater. **12**, 1107 (2013).

12 G. Beaucarne, Adv Optoelectron. **2007**, 1 (2007).

13 Vaughan, David J., and James R. Craig. Mineral Chemistry of Metal Sulfides. Cambridge: Cambridge UP, 1978. Print.

14 V. M. Huxter, T. Mirkovic, P. S. Nair, and G. D. Scholes, Adv. Mater. **20**, 2439 (2008).

15 A. Braga, S. Gimenez, I. Concina, A. Vomiero, I. Mora-Sero, J. Phys. Chem. Lett. **2**, 454 (2011).

16 E. Hirahara, J. Phys. Soc. Jpn. **6**, 422 (1951).

17 R.W. Potter, Econ. Geol. **72**, 1524 (1977).

18 H.T. Evans, Jr., Z. Kristallogr. **150**, 299 (1979).

19 G. Will, E. Hinze, A. Rahman, and M. Abdelrahman, Eur. J. Mineral **14**, 591 (2002).

20 K. Koto and N. Morimoto, Acta Cryst. B **26**, 915 (1970).

21 V. Klimov, P. Haring Bolivar, H. Kurz, V. Karavanskii, V. Krasovskii, and Yu. Krkishko, Appl. Phys. Lett. **67**, 653 (1995).

22 V. I. Klimov and V. A. Karavanskii, Phys. Rev. B **54**, 8087 (1996)

23 P. Lukashev, R.L. Lambrecht, T. Kotani, M. V. Schilfgaarde, Phys. Rev. B **76**, 195202 (2007).

24 Q. Xu, B. Huang, Y. Zhao, Y. Yan, R. Noufi, S.-H. Wei, Appl. Phys. Lett. **100**, 061906 (2012).

25 G. Liu, T. Schulmeyer, J. Brotz, A. Klein, W. T. Jaegermann, Solid Films **477**, 431 (2003).

26 S. Sirivisoot, MRS Bulletin (2008).

27 B.G. Caswell, G.J. Russell, J. Woods, J. Phys. D: Appl. Phys. **8**, 1889 (1975).

28 J. A. Bragagnolo, A. M. Barnett, J. E. Phillips, R. B. Hall, A. Rothwarf, J. D. Meakin: IEEE Trans. Electron Devices ED **27**, 645 (1980).

29 A.M. Dhafiri, G.J. Russell, J. Woods, Semicond. Sci. Technol **7**, 1052 (1992).

30 P. Kumar, R. Nagarajana, R. Sarangi, J. Mater. Chem. C **1**, 2448 (2013).

31 W.D. Gill, R.H. Bube, J. Appl. Phys. **41**, 3731 (1970).

32 L. D. Partain, P. S. McLeod, J. A. Duisman, T. M. Peterson, D. E. Sawyer, and C. S. Dean, J. Appl. Phys. **54**, 6708 (1983).

33 F. Pfisterer, Thin Solid Films **470**, 431 (2003).

34 L. Fotouhi, M. Rezaei, Microchimica Acta **167**, 247 (2009).

35 M. Sam, M.R. Bayati, M. Mojtahedi, K. Janghorban, Appl. Surf. Sci. **257**, 1449 (2010).

36 J. K. labanowski, Simplified and Biased Introduction to Density Functional Approaches in Chemistry, OSC (1996).

37 R. 0.Jones, O. Gunnarsson, Rev. Mod. Phys. **61**, 689 (1989).

38 K. Burke, The ABC of DFT, Rutgers University (2003).

39 O. Gunnarson, H. Hjelmberg, Phys. Scr. **11**, 97 (1975).

40 R. G. Parr, W. Yang, Density-Functional Thoery of Atoms and Molecules (1989).

41 M. Gell-Mann, K. Bruecker, Phys. Rev. **106**, 364 (1957).

42 E. Wigner, Phys. Rev. **46**, 1002 (1934).

43 J. P. Perdew, K. A. Jackson, M. R. Pederson, D. J. Singh, and C. Fiolhais, Phys. Rev. B **46**, 6671 (1992).

44 A. D. Becke, J. Chem. Phys. **98**, 5648 (1993).

45 V. Ozoliņš and M. Körling, Phys. Rev. B **48**, 18304 (1993).

46 E. I. Proynov, E. Ruiz, A. Vela, and D. R. Salahub, Int. J. of Quant. Chem. **56**, 61 (1995).

47 D. Hamann, Phys. Rev. Lett. **76**, 660 (1996).

48 E. Engel and R. M. Dreizler, Density Functional Theory, 1st ed. (Springer Berlin Heidelberg, Berlin, Heidelberg, 2011), p. 19.

49 V. I. Anisimov, J. Zaanen, and O. K. Andersen, Phys. Rev. B **44**, 943 (1991).

50 P. W. Anderson, Phys. Rev. **124**, 41 (1961).

51 T. Bak, J. Nowotny, M. Rekas, and C. C. Sorrell, Int. J. Hydrogen Energy **27**, 991 (2002).

52 M. Cococcioni and S. de Gironcoli, Phys. Rev. B **71**, 1 (2005).

53 J. Heyd, G. E. Scuseria, M. Ernzerhof, J. Chem. Phys. **118**, 8207 (2003).

54 J. Heyd and G. E. Scuseria, J. Chem. Phys. **121**, 1187 (2004).

55 J. Heyd, G. E. Scuseria, M. Ernzerhof, J. Chem. Phys. **124**, 219906 (2006).

56 G. Kresse and J. Furthmüller, Phys. Rev. B **54**, 11169 (1996).

57 G. Kresse, J. Furthmüller, Comput. Mater. Sci. **6**, 15 (1996).

58 P. E. Blöchl, Phys. Rev. B **50**, 17953 (1994).

59 J. P. Perdew, K. Burke, M. Ernzerhof, Phys. Rev. Lett. **77**, 3865 (1996).

60 K. Momma, F. Izumi, VESTA: a Three-Dimensional Visualization System (2011).

61 A. Jain, S.P. Ong, G. Hautier, W. Chen, W.D. Richards, S. Dacek, S. Cholia, D. Gunter, D. Skinner, G. Ceder, K.A. Persson, APL Mat. **1**, 011002 (2013).

62 J. Ghijsen, L. Tjeng, J. van Elp, H. Eskes, J. Westerink, G. Sawatzky, and M. Czyzyk, Phys. Rev. B **38**, 11322 (1988).

63 H. T. Evans, Am. Mineral. **66**, 807 (1981).

64 J. Paier, R. Asahi, A. Nagoya and G. Kresse, Phys. Rev. B **79**, 115126 (2009).

65 S. Chen, X. G. Gong, A. Walsh and S.-H. Wei, Appl. Phys. Lett. **94**, 036601 (2009).

66 C. Harding, V. McKee, J. Nelson, J. Am. Chem. SOC. **113**, 9684 (1991).

67 P. B. Balbuena, P. A. Derosa, J. M. Seminario, J. Phys. Chem. B **103**, 2830 (1999).

68 L.W. Wang, Phys. Rev. Lett. **108**, 085703 (2012).

69 R. B. H. Tahar, T. Ban, Y. Ohya, Y. Takahashi, J. Appl. Phys. **83**, 2631 (1998).

70 J. R. Sambrano, G. F. Nobrega, C. A. Taft, J. Andres, A. Beltran, Surf. Sci. **580**, 71 (2005).

71 R. Long, Y. Dai, B. Huang, J. Phys. Chem. C **113**, 650 (2009).

72 Y. Zhang, J. Yan, G. Zhao, W. Xie, Physica B **405**, 3899 (2010).

73 M. Matthew, M. Gopinath, C. S. Kartha, K. P. Vijaykumar, Y. Kashiwaba, T. Abe, Solar Energy **84**, 888 (2010).

Biographical Information

Prashant Khatri completed his high school from Nepal. After high school he worked as a science tutor for high school students. Then he came to USA for his Bachelor degree. He earned his Bachelor of Science degree in Physics from University of Texas at Arlington with Latin honor Sum-Cum Laude. His undergraduate work was on the use of DFT+U theory on Gallium Phosphide (GaP). He joined graduate school at University of Texas at Arlington after the completion of Bachelor degree. He then continued working on theoretical condensed matter physics group led by Professor Muhammad N. Huda. He has authored a paper titled “Application of attractive potential by DFT + U to predict the electronic properties of materials without highly localized bands”. After completion of Masters in Physics, he is planning to work in the field of science where he can use his research experience and analytical skills properly.